21 December 1964 216-101

STUDY OF POROUS WALL

LOW DENSITY WIND TUNNEL DIFFUSERS

Summary Report

FACILITY FORM 602

N65 17602 (ACCESSION NUMBER)

62 (PAGES)

CR-60951 (NASA CR OR TMX OR AD NUMBER)

1 (THRU)

17 (CODE)

(CATEGORY)

GPO PRICE $ _____

OTS PRICE(S) $ _____

Hard copy (HC) 3.00

Microfiche (MF) .75

Prepared for

George C. Marshall Space Flight Center
Huntsville, Alabama 35812

K. W. Rogers

A. I. Lindsay

and

M. R. Bottorff

Approved by:

Raymond L. Chuan
President

Celestial Research Corporation
1015 Fremont Avenue
South Pasadena, California

ABSTRACT

17602

A theoretical and experimental investigation was made of a porous wall diffuser used with a low density hypersonic nozzle. The Reynolds number range of the experiment varied from 1000 to 20,000 based on the nozzle diameter. At the low Reynolds numbers nearly all of the flow passed through the pores of the diffuser. At the higher Reynolds numbers from 70 to 85% of the flow passed through the throat of the diffuser. The measured pressure recoveries varied from 1 to 10 times the test section normal shock pressure. When models were introduced into the test section stream, the mass flow and pressure recovery of the diffuser were markedly reduced. Although the model used to describe the flow through the porous wall appears incorrect, the theoretical and experimental pressure recoveries and mass flows were in good agreement.

Author

TABLE OF CONTENTS

LIST OF ILLUSTRATIONS

NOMENCLATURE

A - area, ft^2

a - radius, ft

C_f - skin friction coefficient, $\dfrac{\tau_\omega}{\frac{1}{2}\rho_\infty u_\infty^2}$

C_h - Stanton number

C_p - specific heat at constant pressure, $Btu/lb^\circ R$

D - diameter, ft

h - heat transfer coefficient, $Btu/ft^2\text{-}sec^\circ R$

K_n - Knudsen number, mean free path/characteristic length

L - length, ft

M - Mach number

$\dot{m}$ - mass flow rate, slugs/sec

P - static pressure, psf

P_T - total or stagnation pressure, psf

R - gas constant, $ft^2/sec^2\ ^\circ R$

Re - Reynolds number

T - static temperature, $^\circ R$

T_T - total or stagnation temperature, $^\circ R$

u - velocity, ft/sec

v - normal or suction velocity, ft/sec

x - distance along nozzle-diffuser, ft

γ - ratio of specific heats

δ^* - displacement thickness, ft

θ - momentum thickness, ft

NOMENCLATURE (continued)

ρ - density, slugs/ft^3

ϕ - porosity or percent open area

ω - nozzle or diffuser half angle

Subscripts

* - nozzle throat

o - stagnation chamber

1 - test section

2 - diffuser throat

3 - downstream of diffuser throat

∞ - free stream

2d - two-dimensional

aw - adiabatic wall

comp - compressible

inc - incompressible

w - wall

INTRODUCTION

The near free molecular flow regime represents a low density flow regime of great practical interest. In this regime the flow about a body is determined by the character of both intermolecular collisions and molecule-wall collisions. The relative importance of these two types of collisions is primarily dependent upon the Knudsen number (Kn) which is the ratio of the mean free path to the pertinent test object dimension. As the Knudsen number increases a smaller fraction of molecules that rebound from the test object will collide with molecules that are proceeding to the test object, so the incoming stream of molecules becomes less and less dependent upon the test object. In the limit $Kn \longrightarrow \infty$, the incoming stream is independent of the test object, and the flow is completely free molecular.

In order to investigate this flow regime experimentally, it is necessary to provide a facility that is capable of producing a range of mean free paths that are greater than and less than the test object dimensions. Since the typical low density hypersonic boundary layer is one or two orders of magnitude greater than the mean free path it is necessary that the wind tunnel be two or three orders of magnitude larger than the test object in order to obtain reliable results at high Knudsen numbers. Due to this large ratio, the wind tunnel must be large even for models with dimensions on the order of one inch.

This requirement for a large tunnel diameter means that the tunnel pumping system must also be large in terms of volume flow. This results from the large physical size of the tunnel and the presence of the low

momentum flow in the boundary layer. In a typical low density diffuser, the relatively thick boundary layer prevents the attainment of any significant pressure recovery in terms of the test section normal shock pressure recovery. Reducing the boundary layer height should be conducive to increasing the pressure recovery through a diffuser.

Bottorff and Rogers (1963) showed that a nozzle with porous walls could be used to provide some control of the boundary layer height through boundary layer suction. It was found that the boundary layer suction reduced the thickness of the boundary layer and therefore allowed a reduction of the physical size of the nozzle for specified test section conditions.

Previously preliminary experiments by Rogers (1962) showed that a porous nozzle and a porous diffuser could be used to obtain pressure recovery in excess of test section normal shock pressure recovery. Since these levels of pressure recovery would permit one or two orders of magnitude reduction in the pumping speed requirement for a low density wind tunnel, it appeared that this approach might make it economically feasible to develop large low density facilities. The present report is a study of the operational characteristics of porous wall low density diffusers when operated with a low density wind tunnel in the Reynolds number range of 10^3 to 1.2×10^4.

THEORETICAL CONSIDERATIONS OF DIFFUSER PERFORMANCE

Non-Porous Nozzle and Diffuser Walls

In the typical operation of a supersonic wind tunnel (Figure 1), air is expanded from the nozzle throat (Station *) to the test section (Station 1) and compressed from the test section to the diffuser throat (Station 2). The flow becomes subsonic at Station 3. If the flow between the nozzle throat and the diffuser throat were completely isentropic, it would be possible to compress the flow to the sonic condition at the diffuser throat. Assuming the flow was adiabatic, the diffuser throat would be the same size as the nozzle throat. There would be no loss in stagnation pressure through the wind tunnel and this condition would have the minimum possible pumping requirements. In practice, the flow is never isentropic between the nozzle throat and the diffuser throat and frequently it is not adiabatic. Boundary layer flows and shock waves are the two main phenomena that prevent the flow from being isentropic.

The decrease in stagnation pressure resulting from the non-isentropic flow requires that the diffuser throat be larger than the nozzle throat. From the other viewpoint, the maximum attainable area ratio between the nozzle throat and the diffuser throat can be used as a measure of the stagnation pressure loss between the two throats. Assuming the flow at each throat is uniform and one-dimensional, the continuity equation can be used to develop the relationship between the throat conditions. The present development is simplified by considering the case of a nozzle and a diffuser having solid walls so mass flow entering the nozzle throat must pass through the diffuser throat.

$$\rho_2 u_2 A_2 = \rho_* u_* A_* \tag{1}$$

but

$$\rho u = \frac{P}{RT} M \sqrt{\gamma RT} = \frac{P_T}{\sqrt{T_T}} \left(1 + \frac{\gamma - 1}{2} M^2\right)^{-\frac{\gamma + 1}{2(\gamma - 1)}} M \sqrt{\frac{\gamma}{R}} \tag{2}$$

Therefore, neglecting possible changes in γ and R

$$\frac{P_{T_2}}{P_{T_*}} = \frac{A_*}{A_2} \sqrt{\frac{T_{T_2}}{T_{T_*}}} \left[\frac{1 + \frac{\gamma - 1}{2} M_2^2}{\frac{\gamma + 1}{2}}\right]^{\frac{\gamma + 1}{2(\gamma - 1)}} \frac{1}{M_2} \tag{3}$$

$$\frac{P_{T_2}}{P_{T_*}} = \frac{A_*}{A_2} \sqrt{\frac{T_{T_2}}{T_{T_*}}} \left(\frac{A}{A_*}\right)_2 \tag{4}$$

The term $\left(\frac{A}{A_*}\right)_2$ is the area ratio associated with M_2.

The maximum attainable value of $\frac{A_*}{A_2}$ corresponds to choking, so $M_2 = 1$ and $\left(\frac{A}{A_*}\right)_2 = 1$. In this limiting case, the pressure recovery is given by

$$\frac{P_{T_2}}{P_{T_*}} = \frac{A_*}{A_2} \sqrt{\frac{T_{T_2}}{T_{T_*}}} \tag{5}$$

If the flow is adiabatic, $T_{T_2} = T_{T_*}$ and the pressure recovery at a choked diffuser throat is directly proportional to the area ratio between the nozzle throat and the diffuser throat.

This result corresponds to the minimum pressure recovery that can be

obtained at the specified area ratio. This follows from the fact that the sonic condition corresponds to the maximum mass flow per unit area. Therefore with a fixed area ratio, a reduction in pressure recovery would have to be accompanied by a reduction in mass flow. Since the mass flow is fixed by the continuity equation, it is not possible to have a pressure recovery at the throat that is less than that given by Equation 5. There may be significant losses downstream of the throat, so the overall pressure recovery $(\frac{P_{T_3}}{P_{T_*}})$ may be below that given in Equation 5. This is illustrated in Figure 2, which compares the results of Equation 5 with the experimental results reported by Johnston and Witcofski (1960). The experimental pressure recovery exceeds the theoretical value for smaller values of area ratio $\frac{A_*}{A_2}$, but as the maximum experimental values of $\frac{A_*}{A_2}$ are approached, the experimental pressure recoveries fall below the theoretical ones. This is the result of losses downstream of the diffuser throat section.

Figure 2 also emphasizes that experimentally the point of maximum pressure recovery does not correspond to a choked throat. This follows from the prior argument that the maximum mass flow per unit area corresponds to the choking point. Contraction beyond this choking point combined with decreasing pressure recovery is not possible without a corresponding decrease in mass flow. Since the mass flow was constant during the experiments, it follows that the throat was not sonic at the maximum pressure recovery point.

While the analysis based on a sonic diffuser throat is not valid in calculating the overall pressure recovery, it is useful in establishing the minimum pressure recovery that can exist at the diffuser throat. It

is also possible to use the one-dimensional analysis to establish the maximum pressure recovery that can be obtained for a specified area ratio between the nozzle throat and the diffuser throat. This is done by assuming that the flow is isentropic between the two throats. In this case, the flow enters the diffuser throat at a supersonic velocity and the idealized pressure recovery will be that associated with a normal shock at this supersonic diffuser throat Mach number. It can be seen that this is the maximum possible pressure recovery for the specified area ratio by noting that while any consideration of boundary layer displacement effects tends to reduce the Mach number, and therefore the shock losses associated with the flow, the viscous losses associated with the boundary layer growth are greater than the benefit resulting from the lower Mach number.

Equation 4 can be used to calculate the maximum possible pressure recovery. In the equation, M_2 is the Mach number downstream of the normal shock wave. In the limiting case of a very high Mach number upstream of the normal shock, the downstream Mach number becomes

$$M_2 \longrightarrow \sqrt{\frac{\gamma - 1}{2}} \qquad M_{2_{upstream}} \longrightarrow \infty \tag{6}$$

When Equation 6 is substituted into Equation 4 and the results evaluated for $\gamma = 1.4$,

$$\frac{P_{T_2}}{P_{T_*}} = 1.65 \frac{A_*}{A_2} \sqrt{\frac{T_{T_2}}{T_{T_*}}} \tag{7}$$

While this equation is based on the assumption of a very high incoming Mach number, it is within 10% for throat Mach numbers down to $M = 4.2$.

Now Equations 5 and 7 represent two limiting sets of assumptions. Equation 5 is based on the assumption that the stagnation pressure losses are such that the diffuser throat is choked and therefore represents the minimum pressure recovery that can occur at that throat area ratio and temperature ratio.. Equation 7 is based on the assumption that the stagnation pressure is constant to the diffuser throat where the flow becomes subsonic through a normal shock, and therefore it represents the maximum pressure recovery that can occur at that throat area and temperature ratio. Since Equations 5 and 7 only differ by the factor 1.65 it is clear that the pressure recovery is essentially established by the throat area ratio and the temperature ratio and is independent of the processes between the two throats. The processes between the two throats will of course determine the possible throat area ratio and temperature ratio, but the significant point is that if the limiting values of throat area ratio and temperature ratio are established, the maximum throat pressure recovery must fall within the range of Equations 5 and 7. It is to be emphasized that the minimum measured pressure recovery may be below the limits established by Equation 5. This is due to losses occurring downstream of the throat.

Porous Wall Nozzle and Diffuser

It is necessary to determine the effect of the flow through the porous walls when calculating the pressure recovery of a system having porous walls. Since both the nozzle and diffuser walls may be porous, the decrease in mass flow between the nozzle throat and the diffuser throat must be

considered in deriving the porous wall counterparts of Equations 5 and 7.

If the mass flow through the diffuser throat is less than the mass flow through the nozzle throat, Equation 1 can be re-written

$$\rho_2 \, u_2 \, A_2 = \frac{\dot{m}_2}{\dot{m}_*} \, \rho_* \, u_* \, A_* \tag{8}$$

This is the only change due to the suction. The porous wall counterparts of Equations 5 and 7 become Equations 9 and 10, respectively.

$$\left(\frac{P_{T_2}}{P_{T_*}}\right)_{min} = \frac{\dot{m}_2}{\dot{m}_*} \frac{A_*}{A_2} \sqrt{\frac{T_{T_2}}{T_{T_*}}} \tag{9}$$

$$\left(\frac{P_{T_2}}{P_{T_*}}\right)_{max} = 1.65 \, \frac{\dot{m}_2}{\dot{m}_*} \frac{A_*}{A_2} \sqrt{\frac{T_{T_2}}{T_{T_*}}} \tag{10}$$

Thus Equations 9 and 10 are just Equations 5 and 7 multiplied by $\frac{\dot{m}_2}{\dot{m}_*}$.

Thus in order to use these equations in calculating the limits on pressure recovery as a function of area ratio, it is necessary to determine the variation of $\frac{\dot{m}_2}{\dot{m}_*}$ and $\frac{T_{T_2}}{T_{T_*}}$ with area ratio.

The term $\frac{\dot{m}_2}{\dot{m}_*}$ can be obtained if the suction flow through the porous wall can be determined.

$$\frac{\dot{m}_2}{\dot{m}_*} = 1 - \frac{\dot{m}_{suction}}{\dot{m}_*} \tag{11}$$

The temperature ratio $\frac{T_{T_2}}{T_{T_*}}$ cannot be determined in such a direct manner. However, since the pressure recovery varies as the temperature ratio to the one-half power, the accuracy of the temperature ratio is less significant than the accuracy of the mass flow ratio. The temperature ratio can be estimated from the heat transfer to the walls of the nozzle

and the diffuser by the following heat balance.

$$\underbrace{\dot{m}_* C_p T_{T_*}}_{\text{Heat in}} = \underbrace{\int_A h\,(T_{a.w.} - T_w)\,dA}_{\text{Heat transferred to wall}} + \underbrace{(\dot{m}_* - \dot{m}_2)\,C_p\,T_{\text{suction flow}}}_{\text{Heat carried through porous wall}} + \underbrace{\dot{m}_2\,C_p\,T_{T_2}}_{\text{Heat passing through diffuser throat}} \tag{12}$$

This will be simplified by the following assumptions: (1) The Prandtl number is unity so $T_{T_*} = T_{a.w.}$; (2) the wall temperature is constant; and (3) the gas leaves the porous wall at the wall temperature so $T_{\text{suction}} = T_w$. Using these assumptions, the temperature ratio becomes

$$\frac{T_{T_2}}{T_{T_*}} = \frac{\dot{m}_*}{\dot{m}_2}\left[1 - \left(1 - \frac{T_w}{T_{T_*}}\right)\frac{1}{\dot{m}_* C_p}\int_A h\,dA - \left(1 - \frac{\dot{m}_2}{\dot{m}_*}\right) T_w\right] \tag{13}$$

In order to solve this it is necessary to determine the heat transfer coefficient (h).

The Reynolds analogy $C_h = K\,C_f$ can be applied to the present analysis. If the effect of pressure gradient is neglected, the constant K is equal to one-half for a suction boundary layer as well as for a non-suction boundary layer. As will be seen later, the effect of pressure gradient

is small as far as the flow properties are concerned, so this effect will be ignored in calculating the heat transfer rate.

The variation of pressure recovery with area ratio can now be estimated if the local skin friction coefficient and the total mass flow through the pores can be determined. Bottorff and Rogers (1963) presented a technique for calculating the flow properties in a porous laminar flow nozzle. This technique used an iterative procedure which satisfied the momentum and continuity equation at each station in the nozzle. The energy equation was incorporated by assuming a Prandtl number of unity and using the Crocco integral relationship to relate momentum and energy (Crocco, 1948). The local boundary layer characteristics were determined from the suction boundary layer calculations of Iglisch (1949) modified to include the effects of heat transfer, compressibility and axisymmetric boundaries. These characteristics were used to calculate the wall shearing stress, the momentum thickness, the displacement thickness, and the height of the boundary layer.

The flow through the pores was estimated by assuming that the pores were connected to a reservoir containing a gas at uniform conditions. The stagnation pressure for the reservoir gas was assumed equal to the local static pressure in the nozzle and the stagnation temperature of the reservoir gas was assumed equal to the nozzle wall temperature. The effect of pore $\frac{L}{D}$ and Reynolds number was included in the calculation of the pore mass flow. Since this approach provides the flow characteristics necessary to calculate $\frac{\mathring{m}_2}{\mathring{m}_*}$ and $\frac{T_{T_2}}{T_{T_*}}$ in the nozzle, the computer program was modified to include the calculation of the flow into the diffuser.

Starting Limitations

Since the pressure recovery is directly proportional to the ratio of the nozzle throat area to the diffuser throat area, it is important to be able to establish a large value of this ratio. In a solid wall diffuser, the value of this ratio is limited by the starting process. During the starting of a supersonic nozzle, the shock waves must pass through the test section into the diffuser throat. The diffuser throat must be sized to allow all of the relatively low pressure recovery air to pass through the diffuser throat during the starting process. This places a severe limitation on the pressure recovery of a fixed geometry diffuser, and in order to obtain larger pressure recoveries it is necessary to use variable geometry diffusers. Since this is not practical for an axisymmetric diffuser, most axisymmetric diffusers have fixed geometry and limited contraction. While the porous diffuser must operate under a similar limitation, it is in a more favorable position. This results from the fact that the pores, as well as the diffuser throat, are available for the passage of mass flow during the starting process. Thus during the critical phase when the starting shock system is near the test section, the entire porous diffuser and throat are available for mass flow, whereas the solid wall diffuser has only the throat area available. After the porous wall diffuser has started, the low static pressure combined with the supersonic flow field acts to reduce the flow through the pores so that whereas the entire flow could pass through the pores with the shock system at the test section, after the diffuser has started only a fraction of the flow passes through the pores.

In order to calculate the mass flow that passes through the pores of the diffuser during the starting process it is necessary to make several assumptions. These will be discussed in the section on the results of the numerical calculations.

THEORETICAL CALCULATION OF DIFFUSER BOUNDARY LAYERS

General Approach

The method of Bottorff and Rogers (1963) for calculation of compressible laminar boundary layers in nozzles with suction was extended during this study to include calculation of the flow in porous diffusers. The extension assumes that the boundary layer concept can be carried into the diffuser and that the flow in the core is one-dimensional and isentropic. Although this model can only be taken as a rough approximation of the physical case, it was hoped that its results would be useful at least for the prediction of trends. A brief description of this method follows.

The method uses a momentum integral approach to the calculation of the boundary layer characteristics. The velocity at the wall is allowed to be finite to include the effects of suction. Definitions of momentum and displacement thicknesses which account for transverse curvature are used. The solution for the momentum integral equation is

$$\theta_{\infty} = \frac{1}{G(x)} \int_0^x W(x)\, G(x)\, dx \tag{14}$$

where

$$G(x) = \exp \int_0^x \left[\frac{(\delta^*/\theta)_{2d}}{u_{\infty}} \frac{du}{dx} + \frac{1}{a\, \rho_{\infty} u_{\infty}^2} \frac{d}{dx} \left(\rho_{\infty} u_{\infty}^2 a \right) \right] dx \tag{15}$$

and

$$W(x) = \frac{C_f}{2} \sec \omega + \frac{v_w}{u_{\infty}} \frac{T_{\infty}}{T_w} \sec \omega \tag{16}$$

Flat plate values for δ^*/θ and C_f were used in the above equations. These were obtained from an exact solution developed by Iglisch (1949) for incompressible flow. In Iglisch's work, these quantities are functions of the parameter

$$\frac{v_w}{u_\infty}\sqrt{Re_{inc}} \quad . \tag{17}$$

But since

$$Re_{inc} = (Re_{comp})_{wall} = \left(\frac{T_\infty}{T_w}\right)^2 (Re_{comp}), \tag{18}$$

the results of Iglisch can be used directly as functions of

$$\frac{v_w}{u_\infty}\left(\frac{T_\infty}{T_w}\right)\sqrt{Re_{comp}} \tag{19}$$

to get C_f and $\left(\frac{\delta^*}{\theta}\right)_{2d\ inc.}$. The value of $\left(\frac{\delta^*}{\theta}\right)_{2d\ inc.}$ is then used in the following equation (Sivells and Payne, 1959) to get $\left(\frac{\delta^*}{\theta}\right)_{2d}$.

$$\left(\frac{\delta^*}{\theta}\right)_{2d} = \left(\frac{\delta^*}{\theta}\right)_{2d\ inc.} \frac{T_w}{T_\infty} + \frac{T_{a.w.}}{T_\infty} - 1 \tag{20}$$

The parameter $\frac{v_w}{u_\infty}$ was computed by assuming that the flow through the porous wall is choked with stagnation conditions equal to the wall static pressure and temperature. The hole flow coefficients were taken from experimental data for thin orifices over a Reynolds number range from continuum to near free molecule.

Equation 14 must be solved numerically. A program for an IBM 7090 computer was developed and was available for the present study. No account was taken of pressure gradient effects on C_f and $\frac{\delta^*}{\theta}$ in the earlier study.

Modification of Boundary Layer Equations to Include Pressure Gradient Effects

During the present study, an effort was made to include the effects of pressure gradient in the IBM 7090 computer program, because of the possible importance of the adverse pressure gradient in a diffuser.

No solutions were found in the literature for the compressible laminar boundary layer with heat transfer, suction, and pressure gradient. Thus in order to estimate the pressure gradient effect, it is necessary to resort to solutions of the solid wall boundary layer with pressure gradient and apply these as perturbation type corrections to the C_f and $\frac{\delta^*}{\theta}$ values for the suction boundary layer.

Solutions to the laminar boundary layer equations that include the effects of heat transfer, compressibility and pressure gradient have been quite limited in number. The method of Cohen and Reshotko (NACA-TR-1294, 1956), as distinct from other methods, does not require the solution of one or more ordinary differential equations and seemed to be the most suitable for inclusion into the method of Bottorff and Rogers. Cohen and Reshotko, after applying Stewartson's transformation to the boundary layer equations, use Thwaite's concept (developed by him for incompressible flow) of relating the wall shear, its normal derivative at the wall, and the form factor to one another without specifying a type of velocity profile. Non-dimensional forms of these quantities were defined and were evaluated by examining exact solutions for the laminar boundary layer, in this case those of Cohen and Reshotko (NACA-TR-1293, 1956).

The C_f equation developed by Cohen and Reshotko is the following:

$$C_f \sqrt{Re_w} = 2\ell \sqrt{\frac{\frac{x}{u_\infty}\frac{du_\infty}{dx}}{n_p \frac{T_\infty}{T_{T_\infty}}}} \qquad (21)$$

Converting this to the C_f used in Bottorff and Rogers, we have

$$C_f = \frac{2}{\sqrt{Re_\infty}} \frac{T_\infty}{T_w} \sqrt{\frac{\frac{x}{u_\infty}\frac{du_\infty}{dx}}{n_p \frac{T_\infty}{T_{T_\infty}}}} \qquad (22)$$

Cohen and Reshotko have obtained the shear parameter ℓ as a function of the correlation number n_p, which must be known if this method is to be used. If there is no pressure gradient, $n_p = 0$.

Since the Cohen method was not developed for a suction boundary layer, application of its results to a porous nozzle-diffuser are limited to a "perturbation" type of correction to the C_f developed in Bottorff and Rogers for suction boundary layers. Thus a ΔC_f can be defined as

$$\Delta C_f = \frac{2\Delta\ell}{\sqrt{Re_\infty}} \frac{T_\infty}{T_w} \sqrt{\frac{\frac{x}{u_\infty}\frac{du_\infty}{dx}}{n_p \frac{T_\infty}{T_{T_\infty}}}} \qquad (23)$$

where $\Delta\ell$ is the pressure gradient correction to the shear parameter ℓ.

In the case of δ^*/θ, Cohen and Reshotko give the following equation:

$$H = \frac{\delta^*}{\theta} = H_{tr} + \frac{\gamma - 1}{2} M_\infty^2 (H_{tr} + 1) \qquad (24)$$

where H_{tr} is a transformed form factor and is, like C_f, a function of

the correlation number n_p. For no pressure gradient, $H_{tr} = H_{inc} \frac{T_w}{T_{aw}}$. If a pressure gradient exists, H_{tr} can be written

$$H_{tr} = H_{inc} \frac{T_w}{T_{aw}} + \Delta H_{tr} \tag{25}$$

where ΔH_{tr} is the correction due to pressure gradient from Cohen and Reshotko. If H_{tr} is used instead of $H_{inc} \frac{T_w}{T_{aw}}$ in the method of Bottorff and Rogers, the resulting equation for $(\delta^*/\theta)_{2\,d}$ with pressure gradients is:

$$(\delta^*/\theta)_{2\,d} = (H_{tr} \frac{T_{aw}}{T_w} + \Delta H_{tr}) \frac{T_w}{T_\infty} + \frac{T_{aw}}{T_\infty} - 1 \tag{26}$$

Considerations Regarding Separation

In modifying the computer program to include diffuser calculations, the range of the pressure gradient correlation parameter n_p had to be arbitrarily limited to a value below that which would cause separation for a no suction boundary layer. The possible error introduced by doing this may be large, as indicated by Figure 3, where a typical calculated variation of n_p along the diffuser is plotted. It is clear that if the boundary layer actually separates at the point indicated for no suction, diffuser performance will be poor. Although the plot indicates that a no suction diffuser would separate at the entrance, the n_p at this point is not considered valid because it occurs at the nozzle-diffuser boundary. If the boundary layer separates at even the second indicated point, however,

the contraction of the diffuser would be quite limited and the pressure recovery would be essentially that associated with a test section normal shock. It has been found experimentally, however, that this separation apparently does not occur, or if it does occur it fails to seriously disrupt the core flow. This statement is based on the fact that pressure recoveries of up to ten times normal shock were achieved in the tests and also upon the fact that measured diffuser static pressures exhibited a smooth increase along the length of the diffuser.

The separation point indicated on the plot was for a no suction boundary layer. It is well known that boundary layer suction delays separation, so that a higher value of the separation n_p can be expected for a suction boundary layer. Investigations have been made to attempt to determine the magnitude of the increase in the pressure gradient parameter that will be caused by the suction. No references were found relating the effect of suction to the separation pressure gradient parameter in a compressible boundary layer. In view of this lack of information on compressible boundary layers, it was decided to attempt to determine the order of magnitude change in pressure gradient parameter due to suction by using the results of incompressible analysis.

Spalding and Evans have prepared a series of reports that compile the available exact solutions of the incompressible boundary layer with an arbitrary pressure gradient and suction. In their work the suction boundary layer is characterized by parameters such as the momentum thickness, the kinematic viscosity, the local axial velocity gradient, and the suction flow rate. The velocity gradient is assumed to be of the form $\frac{du}{dx} = cu^n$. The sign of the constant c will be positive or

negative, depending upon whether the flow is accelerating or decelerating. For all of the data presented, the exponent n has been limited to values less than 2 for positive velocity gradients and to values greater than 2 for negative velocity gradients (diffusers). The limitations have no physical significance, but are made only for mathematical simplicity. These restrictions are important in the case of hypersonic diffusers, however, since for the velocities of interest in the present study (3000 to 4000 fps) calculations have been carried out only for extreme velocity gradients. It is thus apparent that the incompressible flow calculations are not useful in attempting to determine the magnitude of the effect of suction on the separation point.

Results of Calculations With and Without Pressure Gradient

Figure 4 is a comparison of the computer results with and without the previously described pressure gradient correction. Mach number and $\dot{m}_2/\dot{m}_*$ have been plotted versus the distance along the nozzle-diffuser centerline for the 8° half angle, 15% porosity diffuser at stagnation conditions typical of those used in the tests. The pressure gradient correction gives a lower Mach number at all locations which implies that the increased skin friction coefficient more than offsets the favorable shape parameters and results in an increase in boundary layer thickness. However, it appears that the Mach number difference disappears near the end of the diffuser. Mass flow ratios, however, are about 5% to 15% higher (suction flow 5% to 15% lower) in the no pressure gradient case, a result of the lower tunnel static pressures for this case.

In order to further assess the validity of the Cohen-Reshotko method for calculating laminar boundary layer characteristics in a pressure gradient, the nozzle boundary layer was calculated for the pressure gradient and no pressure gradient cases for an existing $M = 6$ nozzle which has been thoroughly investigated experimentally. The comparison between the resulting test section Mach numbers is shown in Figure 5. Again, the pressure gradient case shows a decreased Mach number and is in poorer agreement with experiment than the no pressure gradient calculations.

It appears that the Cohen-Reshotko procedure may over-estimate the effect of the pressure gradient on the skin friction coefficient. This is also implied in a report by Carden who compared experimentally measured heat transfer coefficients in a laminar flow nozzle with the results of calculations using the Cohen-Reshotko procedure. The heat transfer coefficients calculated by the Cohen-Reshotko procedure greatly exceed experimentally determined ones. In view of this uncertainty of the adequacy using the Cohen-Reshotko procedure to calculate the effect of pressure gradient on nozzle-diffuser boundary layer characteristics and also considering that the effect of the pressure gradient appears small when used in the calculation of the nozzle-diffuser boundary layer, it is concluded that for the purposes of this study the effects of pressure gradient can be neglected.

RESULTS OF THEORETICAL CALCULATIONS

Mass Flow

Calculations were made for a series of nozzle-diffuser combinations. The variables included the Mach number, the Reynolds number, the contraction angle ω , and the porosity ϕ . While the important parameters in determining the performance of a diffuser are the pressure recovery and mass flow relationships, by the use of Equations 9 and 10 it is possible to determine the limits on pressure recovery if the variation of mass flow and temperature ratio with area ratio are known. Figures 6 through 8 show the typical variation of mass flow ratio with diffuser area ratio.

The porous nozzle used in these calculations had a 26° included angle and a 12" exit diameter. The nozzle throat was varied between Mach number 10 and Mach number 6. Both the nozzle and the diffuser walls were at liquid nitrogen temperature. The lowest values of $\frac{A_*}{A_2}$ are those corresponding to the test section.

Figure 6 shows the variation of mass flow with area ratio for different values of ϕ and ω . From this plot it is seen that increasing either the porosity or the length increases the flow through the pores. This is consistent with what would be expected intuitively, i.e., that the flow out the diffuser wall would be approximately proportional to the total open area of the diffuser. The total flow through the diffuser pores is not directly proportional to the area of the diffuser pores because increasing diffuser pore flow results in decreasing static pressures in the diffuser. Since the local mass flow through the diffuser pore is almost directly proportional to the local static pressure, the decrease

in static pressure results in a decrease in mass flow per unit open area. This assumed relationship between local mass flow and local static pressure keeps the flow from being directly proportional to the total open area of the diffuser.

Figures 7 and 8 show the effect of Reynolds number on the diffuser performance. Increasing Reynolds number results in a relative reduction in mass flow through the pores. This is due to the increase in Mach number that is associated with an increase in Reynolds number. The Mach number increases because of the reduction in boundary layer height with increasing Reynolds number. The increased Mach number results in a relatively lower static pressure at the pores, and since the pore flow is directly proportional to the static pressure, this results in a reduction in pore flow. As the Reynolds number increases, the boundary layer becomes thinner so the variations in the height of the boundary layer have a smaller effect on the Mach number and pressure in the nozzle and diffuser.

Heat Transfer

In order to use Figures 6 through 8 in calculating the pressure recovery, it is necessary to determine the variation of $\frac{T_{T_2}}{T_{T_*}}$. Calculations were made using the procedure outlined on pages 9 -10 . It was found the heat transferred between the nozzle throat and the diffuser throat was relatively constant and equal to about 15% of the energy entering the nozzle throat. Thus the temperature ratio $(\frac{T_{T_2}}{T_{T_*}})$ is about .85. Since only a small fraction of the energy is transferred from the incoming

gas to the nozzle walls, it is apparent that the temperature ratio is not an important parameter in calculating the theoretical limits on the pressure recovery.

Cryopumped Diffusers

In a low density wind tunnel with porous diffuser, the flow through the pores generally represents a very large volume flow rate because of the low pressures (typically of the order of 1 micron) which must be maintained outside the nozzle and diffuser walls. Thus a cryopump, which can be arranged so that it entirely surrounds the nozzle and diffuser, is an especially attractive means of pumping the suction flow because of the very high pumping speeds which can be achieved.

The cryopump is however a mass flow limited pump and thus the problem in such an installation is to design a diffuser which will minimize the volume flow rate at the diffuser throat while maintaining the pore mass flow below the capacity of the cryopump. To illustrate the trade off involved, calculations were made for the 12° half angle, 15% porosity diffuser with the 12" diameter Mach 10 nozzle. The test section unit Reynolds number was 340/in (P_{T_o} = 1.96 psia, T_{T_o} = 1320°R). Figure 9 presents the maximum possible pressure recovery (Equation 10) and the diffuser throat mass flows as a function of nozzle to diffuser throat area ratio. As the diffuser area ratio is increased the assumed normal shock occurs at a lower Mach number. The lowered Mach number more than offsets the decreased mass flow ratio to give a steadily increasing pressure

recovery as the area ratio is increased. Figure 10 presents the corresponding pumping speed requirements for the diffuser throat flow along with the cryopump capacity required to pump the pore flow. It can be seen that the diffuser throat volume flow can be diminished to very small values but the cryopump capacity curve rises steeply as this is done.

It is apparent then that a trade off must be made to balance the two requirements. The most economical contraction ratio cannot be derived in general terms since it depends on a great many factors (Reynolds number range, tunnel size, availability of various pumping means, etc.) which must be individually considered for each installation.

Starting Calculations

The porous diffuser can start with greater amounts of contraction than a solid wall diffuser since the openings in the diffuser wall that are downstream of the shock system act as additional diffuser throat area during the starting process. These pores are not carefully shaped nozzles but are sharp-edged orifices, so instead of flowing full of gas at a sonic condition, they flow at a lower rate. While, if the pressure ratio is high enough, the flow rate can be estimated as a function of Reynolds number, due to other uncertainties it is adequate to assume the pores are choked.

The temperature of the gas passing through the pores is unknown since it is difficult to estimate the heat transfer. It was found that the heat transfer in the diffuser is low if the diffuser is supersonic

$\left(\frac{T_{T_2}}{T_{T_*}} \approx .85\right)$; however, if the gas is subsonic and at a higher pressure level, the heat transfer will be increased. In view of this uncertainty, a conservative assumption has been made, i.e., the gas is all at the stagnation temperature.

The other major uncertainty is the pressure recovery of the gas behind the normal shock system. At high Reynolds numbers, it has been found experimentally that this shock system has a lower loss than a single normal shock. This is evidenced by the ability of diffusers to start with greater contraction than theory predicts. For the present analysis it has been assumed that these errors are self-compensating, i.e., the reduction in area is just balanced by the higher pressure recovery and lower temperature. Now the starting criteria will be that the quantity of gas that can flow through the open area downstream of the shock wave must equal or exceed the quantity of gas entering the shock wave. The gas flowing through the pores is assumed to be choked at the stagnation temperature and pressure associated with a normal shock. The starting characteristics of several nozzle-diffuser configurations were investigated using this approach. It was found that the crucial phase of the starting process occurs when the normal shock is positioned at the test section. This is the same result that is found for a non-porous diffuser.

EXPERIMENTAL PROGRAM

Facility Description

The experiments were conducted in the Hyperaltitude Facility of the Environmental Division of the U. S. Naval Missile Center, Point Mugu, California. A complete description of this facility is given in Bottorff (1964) and only a brief summary will be presented in this section. The basic facility consists of a 10' diameter 20' long vacuum chamber that has a combination of pumping systems. The primary pumping unit for the present test was a 20°K cryopump that is cooled by a 350 watt gaseous helium refrigerator. The condenser can be isolated from the main chamber by a large 5' diameter valve which allows access to the models and tunnel without bringing the cryopump up to ambient temperature.

The present investigation utilized the porous wall nozzle described in Bottorff and Rogers (1963). This nozzle is basically a Mach 10 nozzle with 12" exit diameter which has liquid nitrogen cooled porous walls.

Experimental Arrangement

The experimental arrangement used in this test is illustrated in Figure 11. The nitrogen gas which was obtained by vaporizing liquid nitrogen was metered into the stagnation chamber to maintain a selected stagnation pressure. After passing through the nozzle throat, part of the flow was removed through the liquid nitrogen cooled porous walls of

the nozzle and the diffuser. This flow passed through the 5' diameter valve into the cryopump. The remaining flow passed through the diffuser throat into the pumping system where it could be directed to either the mechanical pump or the cryopump. The pressure at the end of the diffuser was varied by manipulating the throttle valves (1 and 2).

It was originally planned to use the section M (Figure11) as a metering run; however, this did not prove practical due to erratic pressure drops in the metering section. This erratic performance resulted from the persistence of the core flow when the diffuser throat was supersonic. This problem was alleviated by installing the stilling chamber S (Figure 11) and using the thin-walled orifice as a metering system. In order to use this metering system, it was necessary that all of the flow pass through the stilling chamber and into the cryopump so valve 2 was closed at all times.

Instrumentation

Since there are extremely wide variations of pressure level in the hypersonic wind tunnel, it is necessary to use a variety of pressure gauges to monitor the flow conditions.

The stagnation chamber pressure was measured using a Bourdon gauge which was limited by reading accuracy to 3% to 5% accuracy. The static pressures in the converging section of the supersonic diffuser were measured using thermocouple gauges. The first two instruments had a usable range of 0-100 microns, while the third gauge had a range of 5-1000 microns. By the use of suitable valving, the test section normal

shock pressure, the static pressure in the diffuser throat, and the diffuser recovery pressure were measured using one Alphatron gauge. When it was necessary to measure the static pressure near the diffuser recovery tube, the same Alphatron was used. The pressure in the metering system was measured using a capacitance type mechanical diaphragm gauge. All gauges were calibrated on a device that metered known increments of gas into a container of a fixed and known volume.

Diffuser Configurations

Three diffuser contraction sections were tested. Two contractions had an 8° half angle and the third had a 12° half angle. One 8° diffuser and the 12° diffuser had a porosity of 15%, i.e., there was 15% open area. The second 8° diffuser had a porosity of 30%. The pores consisted of $\frac{1}{4}$" diameter holes drilled in the $\frac{1}{16}$" diffuser wall. The diffusers were constructed so the diameter of the throat section could be varied between 2 inches and $3\frac{1}{2}$ inches. The $\frac{L}{D}$ of the throat was essentially constant at a value of 4.8. The entire diffuser assembly could be moved relative to the nozzle so the effect of varying the free-jet length could be investigated. The supersonic contraction section and the constant area throat were cooled to liquid nitrogen temperature.

The configurations are identified by a code consisting of (1) diffuser half angle,(2) porosity, (3) throat diameter, and (4) free-jet length. Thus 8°-15%-2"-6" refers to the 8° half angle, 15% porosity diffuser with a 2" diameter throat and a free-jet length of 6".

A traverse mechanism was installed so various models could be inserted in the stream. Since these were expected to be high performance diffusers, it was anticipated that the disturbances caused by the models would seriously affect the diffuser performance. The models included a 1" diameter sphere, a 30° included angle cone with a 1" base diameter, and a $\frac{1}{4}$" stagnation pressure probe.

Testing Procedure

During typical testing, the tunnel conditions were established by raising the stagnation chamber pressure to the desired level with the throttle valve wide open. After the pressures had stabilized, the readings were taken and the throttle was closed to raise the pressure at the end of the diffuser section. Typically the valve was closed until the metering system showed a decrease in mass flow and then the valve was opened until the entire mass flow was once more passing through the metering section. This point would roughly correspond to the critical point of the diffuser. Additional data points were then taken with the valve closed beyond this point. This procedure generated plots of pressure recovery versus mass flow that are comparable to those obtained during the testing of supersonic inlets.

It was found that some configurations would not operate properly because of the losses in the 4" diameter metering piping. Since the mass flow data was the most important data, the metering system was shortened and the valves were removed in an attempt to reduce the losses through the metering system. For these configurations only a single mass flow point was obtained for each Reynolds number.

Data Reduction

The pressure data was reduced to coefficient form by ratioing the pressures to the stagnation chamber pressure.

The mass flow through the metering system was obtained by assuming the flow characteristics of the orifice were the same as those reported by Liepmann (1960). In that investigation, an orifice with an $\frac{L}{D}$ of $\frac{1}{40}$ was tested from the continuum range through the free-molecular flow range. Liepmann found that if the Knudsen number of the orifice was below .1, the mass flow was essentially independent of Knudsen number and equal to 85% of the flow that would pass through a sonic throat of the same area. The present experiments were in the same Knudsen number range; however, it was not possible to maintain the same pressure ratio across the orifice. Liepmann maintained a pressure ratio of 1,000. However, he points out in the theoretical development that in continuum flow a pressure ratio of approximately 26 is sufficient to prevent the downstream pressure from influencing the flow through the orifice if the gas has a value of $\gamma = 1.4$. This condition was met for most of the configurations tested in the present investigation.

The relationship between the flow through the nozzle and the flow through the diffuser throat is given by

$$\frac{\dot{m}_2}{\dot{m}_*} = .85 \frac{P_{T_c}}{P_{T_o}} \sqrt{\frac{T_{T_o}}{T_{T_c}}} \frac{A_c}{A_*} \qquad (27)$$

In the present investigation it was found that with room temperature gas entering the nozzle, the temperature of the gas leaving the orifice was

also room temperature. The orifice diameter was 4 inches and the nozzle throat diameter was $\frac{9}{32}$ inch. Equation 27 becomes

$$\frac{\dot{m}_2}{\dot{m}_*} = 172 \frac{P_{T_c}}{P_{T_o}} \tag{28}$$

This is the expression that was used in calculating the diffuser throat mass flow ratio from the measured pressures.

EXPERIMENTAL RESULTS AND COMPARISON WITH THEORY

Pressure Recovery Data

Figure 12 is a plot of measured pressure ratio versus measured mass flow ratio for the diffuser configuration 8°-15%-2"-0. This figure can be used to demonstrate some of these salient features of the experimental results.

The flagged symbols correspond to the pressure recovery measured by the stagnation pressure probe at the end of the diffuser. The plain symbols correspond to the static pressure measured just downstream of that location. The numbers on the points correspond to the sequence of closing the mass flow valve. While the static pressure measured at the aft end of the diffuser follows the theoretical trend insofar as the pressure rises as the valve is closed, the stagnation pressure often does not. This is because the single stagnation pressure tube is generally not representative of the flow conditions at that station. Since the probe is mounted in the center of the tube it is unduly influenced by the high stagnation pressure core which persists into this region when the throttle valve is relatively wide open. As the valve is closed the shock system is moved forward and promotes better mixing so the stagnation pressure probe becomes more representative of the flow at that location.

As the shock system is moved forward the diffuser mass flow begins to decrease. This is probably the result of separation and reversed flow on the walls of the diffuser throat. This separation feeds far enough forward to influence the static pressure measurements in the converging section of the supersonic diffuser.

Due to the fact that the disturbance feeds forward such a long distance, the peak pressure recovery is not obtained until a considerable part of the mass flow is being spilled at the low Reynolds numbers. While this could probably be corrected by using a longer constant area throat, the main benefit would be the increased mass flow at the critical point, since the increase in pressure recovery would be modest. This is clear from the comparison of the experimental pressure recovery with the theoretical maximum possible pressure recovery. The maximum theoretical pressure recovery is obtained by the intersection of vertical lines through the maximum measured mass flows and the line labeled Equation 10. This corresponds to isentropic flow between the nozzle throat and the diffuser throat and therefore represents the maximum possible pressure recovery. The maximum experimental pressure recoveries are within 10 to 15% of the theoretical values.

The agreement between the values of pressure recovery suggests that the relatively short constant area diffuser throats are adequate if some spillage is allowable. If the diffuser walls were solid so mass flow could not be spilled without causing the diffuser to become unstarted, the pressure recovery would be significantly reduced. Under these conditions the maximum pressure recovery would be limited to the values corresponding to the point at which the diffuser throat mass flow starts to decrease.

Figure 13 illustrates the change in diffuser effectiveness caused by opening the free-jet to 6 inches and by installing a model. In order to avoid the erratic pressures measured by the stagnation pressure probe, the pressure ratios were obtained using the static pressure at Station 3.

For most configurations this pressure is within 10% of the stagnation pressure at the peak pressure recovery.

The 6 inch free-jet causes a slight reduction of the mass flow and pressure recovery. The model has a more deleterious effect on the performance, causing significant reductions in mass flow and pressure recovery.

Figures 14 and 15 compare the same performance parameters for configurations 8°-30%-2 and 12°-15%-2.5 , respectively. These configurations show similar characteristics to the ones previously discussed.

It was not always possible to obtain continuous data as the mass flow was reduced by closing valve 1 . As the mass flow was reduced a point was often reached where the shock wave would move abruptly from near the diffuser throat to a point far upstream of the diffuser throat. This would result in negligible values of pressure recovery and mass flow. It appears that under these circumstances the suction was insufficient to stabilize the shock wave system at that point in the diffuser.

Similarly it was not always possible to obtain data at the higher Reynolds numbers. For example, the configuration 12°-15%-3"-6" would not remain started above Reynolds number/inch = 800. As the stagnation pressure was raised above this point, the shock system would abruptly move upstream from the diffuser throat. Since this configuration had a pressure recovery that was comparable to the pressure required to overcome the losses in the metering system, it is possible that the metering system losses were acting as a partially closed valve and forcing the shock system forward of the diffuser throat. In this case, the same mechanism would be involved in the abrupt movement of the shock wave. In one case the crucial condition is achieved by varying the mass flow throttle,

while in the other case it is achieved by raising the stagnation pressure.

From a comparison of the experimentally determined variation of pressure recovery with mass flow and the theory given by Equations 9 and 10, it is apparent that the theory serves as adequate limits to diffuser performance.

Mass Flow Data

Since the data presented so far has confirmed the validity of the limits set by Equations 9 and 10, the remainder of the discussion will be concerned with mass flow ratios. Figures 16 through 19 illustrate the variation of mass flow ratio with Reynolds number for the various configurations. The theoretical test section mass flow is included to indicate the magnitude of the flow through the nozzle pores.

Figures 16, 17 and 18 compare the mass flow characteristics of a series of configurations which only differ by the diameter of the constant area throat. It is seen that the 2" diameter throat and the 3" diameter throat both follow the theoretical trend while the $3\frac{1}{2}$" diameter throat has a lower mass flow than expected. This reduced mass flow was caused by excessive losses in the mass flow metering system which prevented the $3\frac{1}{2}$" configuration from starting properly. This is illustrated by Figure 20, which shows the measured static pressures in the converging section of the diffuser for the three configurations. The $3\frac{1}{2}$" configuration shows a distinct rise in the static pressure before the throat. This pressure rise increases the flow through the pores and results in a lowered mass flow

at the diffuser throat.

Figures 16 and 19 are the same configuration except for an increase in porosity. It is seen that the increased porosity had a small effect on the flow rate in the diffuser. This is in contrast to the theory, which predicted a significant increase in flow rate through the pores. It was found that the configuration with increased porosity had a lower static pressure distribution along the converging section of the diffuser. This lowered static pressure would yield a reduced mass flow rate compared to the 15% configuration. It will be shown in a later section that while the level of the static pressure does not appear to be a satisfactory indication of the flow through the pores, it appears that the variation of the static pressure does coincide with the variation of mass flow. This is borne out by the changes which occurred when a model was introduced into the stream. The introduction of the model caused very high flow rates through the pores and a significant increase in static pressure was measured along the converging section of the diffuser.

In general, the theoretical and experimental flow rates are in good agreement for the configurations with no free-jet. The six inch length of free-jet reduced the mass flow by 5 to 10% for most configurations. The introduction of the model caused a significant reduction in mass flow at all Reynolds numbers, but the influence was most pronounced at the low Reynolds numbers.

The agreement between the theoretical and the experimental values of mass flow must be regarded as somewhat fortuitous, since the measured static pressures in the contraction section of the diffuser were significantly above the theoretical values in all cases. Figure 20 is typical of

this comparison. In the theoretical analysis the out-flow through the pores was assumed to be nearly proportional to the local static pressure. It would be expected that the increased static pressure would result in a much higher pore mass flow rate than that predicted by the theory, which used lower static pressures. This would reduce the mass flow rate through the diffuser throat compared to the theory. For example, if a calculation is made of the pore flow using the experimentally measured pressures (Figure 20) instead of the theoretical values, the mass flow through the pores would be more than doubled. This did not occur experimentally and no explanation has been found for this behavior.

A limited investigation was made of the effect of varying the chamber pressure. It was found that some configurations were unusually sensitive to small chamber pressure variations. For example, during typical operation the chamber pressure varied between $\frac{1}{2}$ and 2 microns, depending upon the flow rate. The pressure was limited by the conductance of the 5' diameter valve which leads to the cryopump. It was found that raising the chamber pressure by 1 micron could cause a significant change in mass flow and pressure recovery. This is illustrated in Figure 21 which shows the variation in diffuser throat mass flow with chamber pressure for a configuration with and without a model installed. Since the pressures measured on the inside of the diffuser were of the order of 10 microns or greater, it is difficult to understand how a chamber pressure variation of 10% of this value would cause such a large change in mass flow. It seems possible that the phenomenon that is responsible for this variation of pore flow with chamber pressure may also be responsible for the reduced

values of pore flow when compared to the theoretical values associated with the high static pressure levels measured in the diffuser.

COMPARISON WITH PREVIOUS EXPERIMENTS

Rogers (1962) presented the results of an experimental investigation of a porous cooled diffuser. In these experiments an attempt had been made to fabricate a variable porosity diffuser. This was done using two porous concentric cones. Due to a difficulty in maintaining alignment between the pores, the level of porosity was not accurately established. A further difficulty was encountered because only the outer cone was cooled with liquid nitrogen. The cooling on the inner cone depended upon conduction from the outer cone. In the present analysis it has been assumed that the wall was cooled to liquid nitrogen temperatures. The effective porosity was determined by making calculations for a series of porosities and selecting the one that agreed with the experiments at a specific Reynolds number. It was found that whereas the porosity of the individual cones was 30%, the effective porosity was 7.5%. The comparison between the theoretical and experimental variation of mass flow with Reynolds number is shown in Figure 22. The porosity had been selected to agree with the experiment at $Re/in = 1000$. It is seen that there is general agreement at all Reynolds numbers except the highest. This highest Reynolds number point is somewhat questionable since the flow leaving the nozzle exit was non-uniform and had strong compressions on the outer edge. While it would be expected that the strong compressions would raise the static pressure and consequently the flow out through the pores of the diffuser, this does not appear to have been the case. The mass flow passing through the diffuser throat was greater than that predicted

by the theory, which indicates a lower mass flow passing through the pores. This is another example of the difficulty of calculating the flow through the pores.

Figure 23 shows a comparison between the theoretical and experimental values of pressure recovery. In this case, Equations 9 and 10 have been used to calculate the limits on the pressure recovery but the experimentally measured mass flow has been used in place of the theoretical value. The results show the experimental pressure recoveries are slightly below the minimum theoretical values. This is the result of losses occurring downstream of the throat of the diffuser.

This diffuser configuration was also adversely affected by the presence of the model in the test section. When a cylinder was inserted into the stream so it spanned the tunnel, the mass flow was decreased by approximately one-half. The cylinder had a diameter equal to about 6% of the test section diameter.

CONCLUSIONS

The results of the series of investigations on porous wall low density wind tunnel diffusers have shown good agreement between theory and experiments. It was predicted theoretically and confirmed experimentally that the limits on the pressure recovery at the diffuser throat can be given by the following simple equation.

$$\frac{P_{T_2}}{P_{T_*}} = C \frac{\dot{m}_2}{\dot{m}_*} \frac{A_*}{A_2} \sqrt{\frac{T_{T_2}}{T_{T_*}}} \qquad (29)$$

In this expression the constant c is unity as a lower limit and 1.65 as an upper limit for hypersonic flow with $\gamma = 1.4$. The lower limit corresponds to choking at the diffuser throat while the upper limit corresponds to isentropic flow between the nozzle throat and the diffuser throat followed by a normal shock. From an analysis of several nozzle-diffuser combinations, it was concluded that the heat transferred to the walls was small and the term $\frac{T_{T_2}}{T_{T_*}}$ would not vary significantly from .85.

From a comparison of the results of a computer program and the experimental investigation, it was found that the theory accurately predicted the variation of diffuser throat mass flow with diffuser throat area ratio. It was concluded, however, that this agreement was somewhat fortuitous since the level of static pressure in the diffuser was much higher than the theoretical value. This higher static pressure should have resulted in an increased mass flow out through the porous walls of the diffuser and a resultant decrease in mass flow through the diffuser

throat. Since this was not found to be the case, it was concluded that the model used in calculating the flow through the diffuser pores was incorrect. It is suggested that this is an area that warrants further study.

It was found that introducing a model into the stream caused a significant reduction in diffuser throat mass flow and pressure recovery. The large decrease in diffuser throat mass flow implies an increase in mass flow through the porous walls. It was found that the diffuser static pressures increased when the model was installed. This would lead to an increase in flow through the porous walls if the flow is proportional to the static pressure.

The theoretical investigation indicated it was possible to obtain pressure recoveries approaching unity for the flow remaining in the diffuser throat. These high pressure recoveries could only be obtained at the expense of having most of the flow pass through the porous walls of the diffuser. Since any practical design must consider the quantity of flow passing through the diffuser pores as well as the flow passing through the throat, it is necessary to make a trade off between diffuser throat pressure recovery and pore mass flow.

REFERENCES

Bottorff, M. R., (1964), "Description and Operating Procedures for the Hyperaltitude Facility at USNMC, Point Mugu, California"

Bottorff, M. R., and Rogers, K. W. (1963), "Theoretical and Experimental Investigation of Boundary Layer Control in Low-Density Nozzles by Wall Suction and Cooling," USCEC Report 90-101.

Carden, William H., (1964), "Local Heat-Transfer Coefficients in a Nozzle with High-Speed Laminar Flow," AEDC-TDR-64-61.

Cohen, Clarence B., and Reshotko, Eli, (1956), "Similar Solutions for the Compressible Laminar Boundary Layer with Heat Transfer and Pressure Gradient," NACA-TR-1293.

Cohen, Clarence B., and Reshotko, Eli, (1956), "The Compressible Laminar Boundary Layer with Heat Transfer and Arbitrary Pressure Gradient," NACA-TR-1294.

Crocco, Luigi, (1948), "The Laminar Boundary Layer in Gases," Rep. CF-1048, Aerophysical Lab, North American Aviation, Inc.

Iglisch, R., (1949), "Exact Calculation of Laminar Boundary Layer in Longitudinal Flow Over a Flat Plate with Homogenous Suction," NACA TM 1205.

Johnston, Patrick J., and Witcofski, Robert D., (1960), "Effect of a Variable-Geometry Diffuser on the Operating Characteristics of a Helium Tunnel Designed for a Mach Number in Excess of 20," NASA-TN-D-237.

Liepmann, H. W., (1960), "A Study of Effusive Flow," reprinted from Aeronautics and Astronautics, GALCIT Publication No. 486.

Rogers, K. W., (1962), "Preliminary Experiments on a Low-Density Hypersonic Wind Tunnel Using a Cooled Porous Nozzle and Diffuser," USCEC Report 65-48, University of Southern California Engineering Center.

Sivells, J. D., and Payne, R. G., (1959), "A Method of Calculating Turbulent-Boundary-Layer Growth at Hypersonic Mach Numbers," AEDC-TR-59-3.

Spalding, D. B., and Evans, H. L., (1960), "Mass Transfer through Laminar Boundary Layers - 2. Auxiliary Functions for the Velocity Boundary Layer," Int. J. Heat Mass Transfer, Vol. 2, pp. 199-221, Pergamon Press 1961.

Spalding, D. B., and Evans, H. L., (1960), "Mass Transfer through Laminar Boundary Layers - 3. Similar Solutions of the b-Equation," Int. J. Heat Mass Transfer, Vol. 2, pp. 314-341, Pergamon Press 1961.

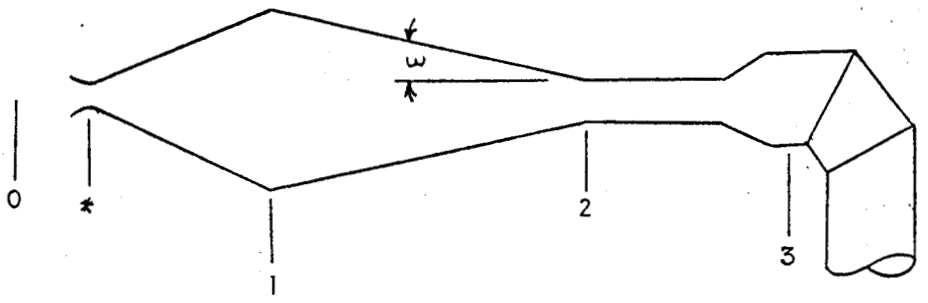

Figure 1. Wind Tunnel Schematic

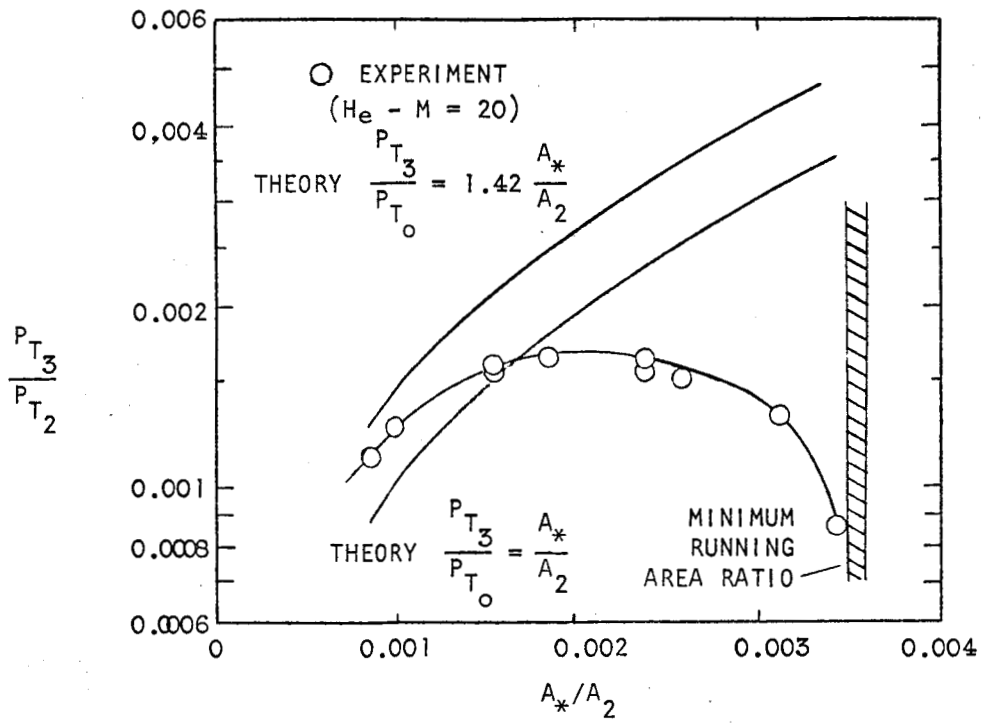

Figure 2. Typical Experimental Diffuser Performance

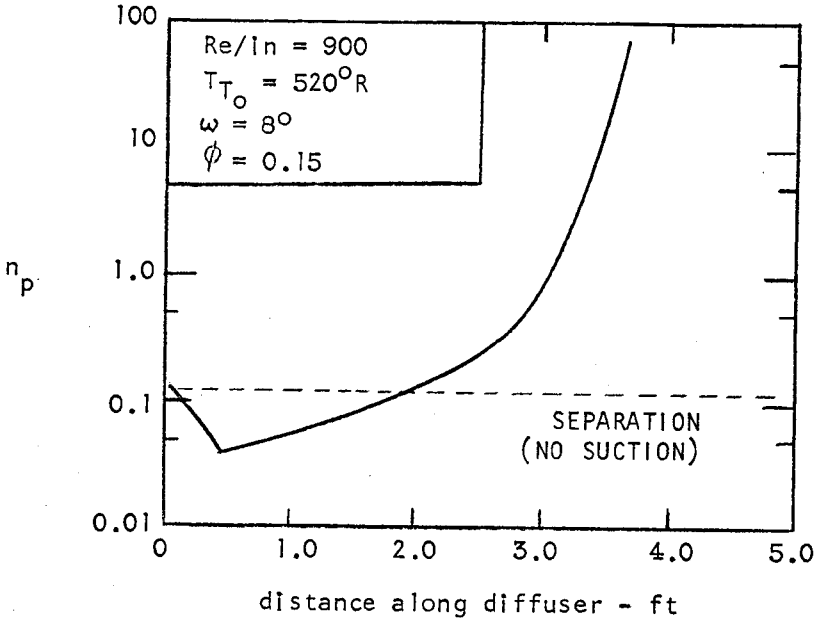

Figure 3. Variation of Pressure Gradient Parameter

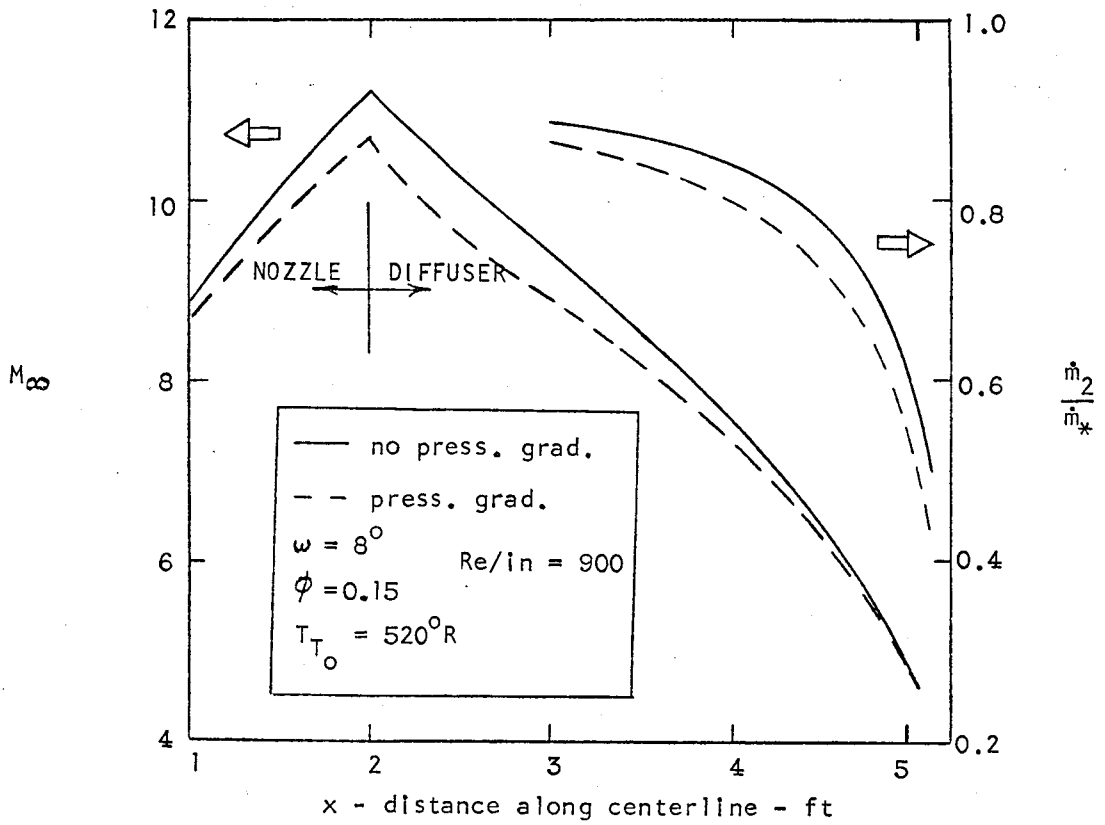

Figure 4. Effect of Pressure Gradient on Mach No. and Mass Flow

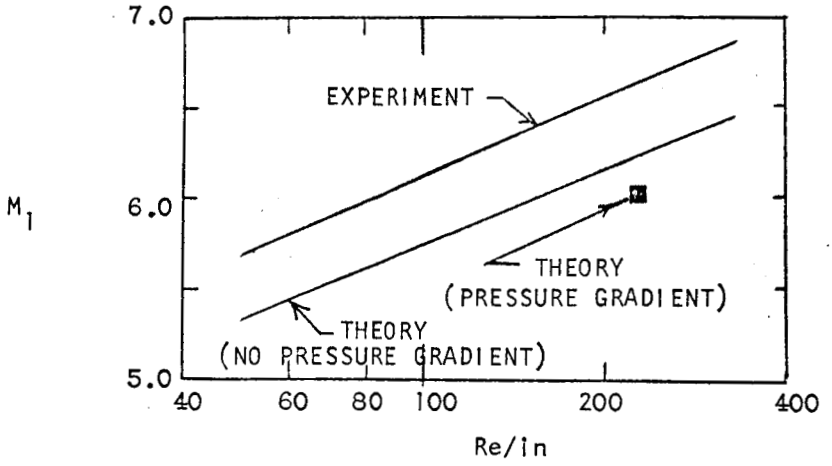

Figure 5. Comparison Between Theoretical and Experimental Mach Numbers.

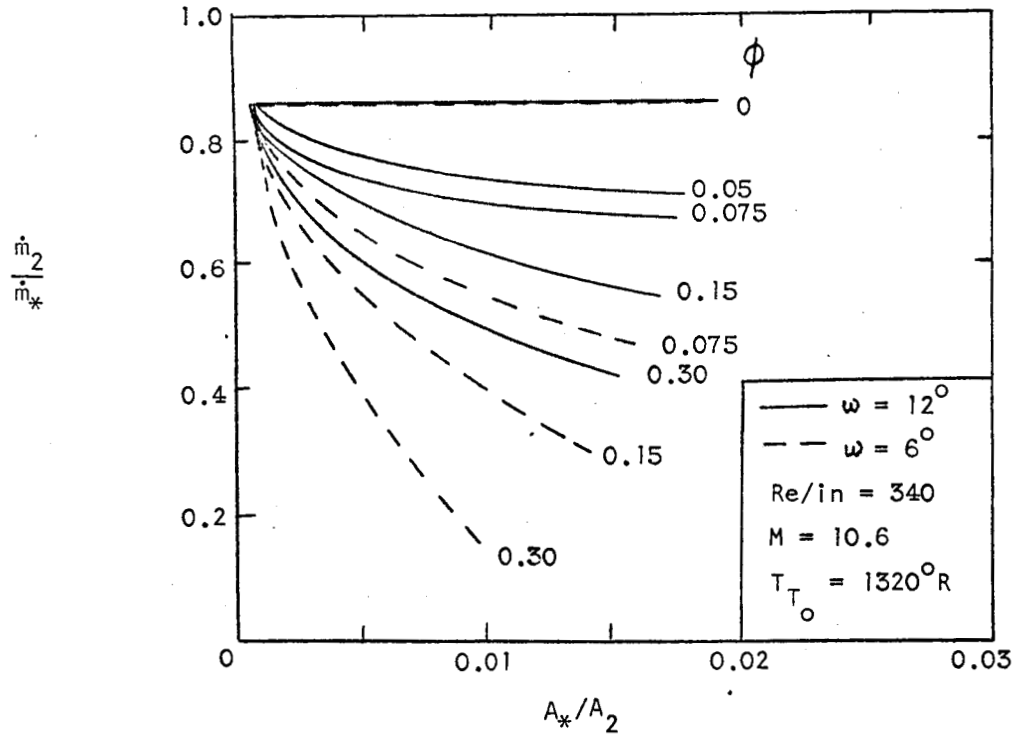

Figure 6. Variation of Diffuser Mass Flow

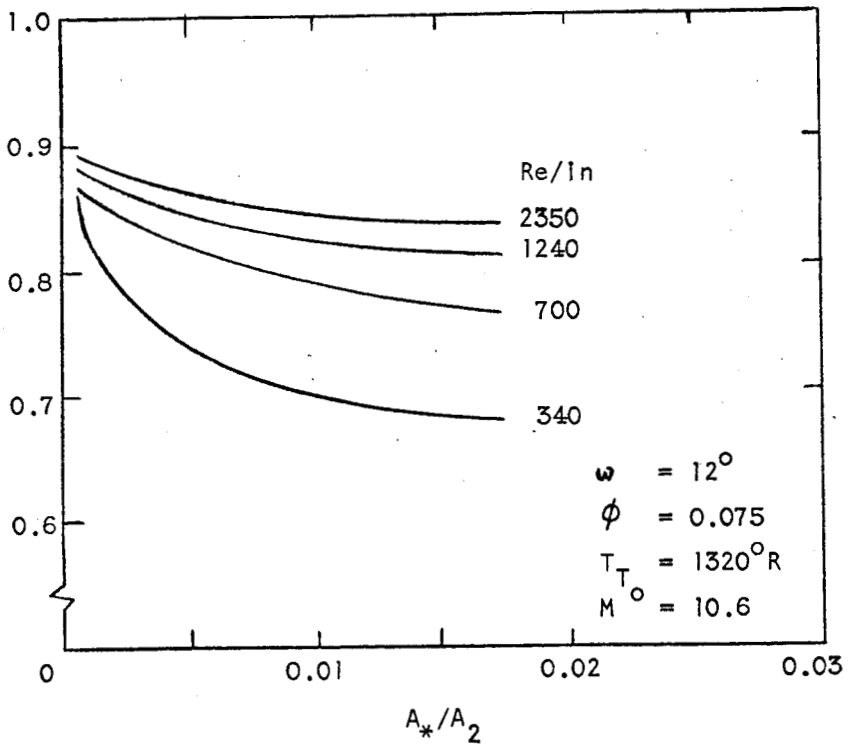

Figure 7. Variation of Diffuser Mass Flow with Reynolds No.

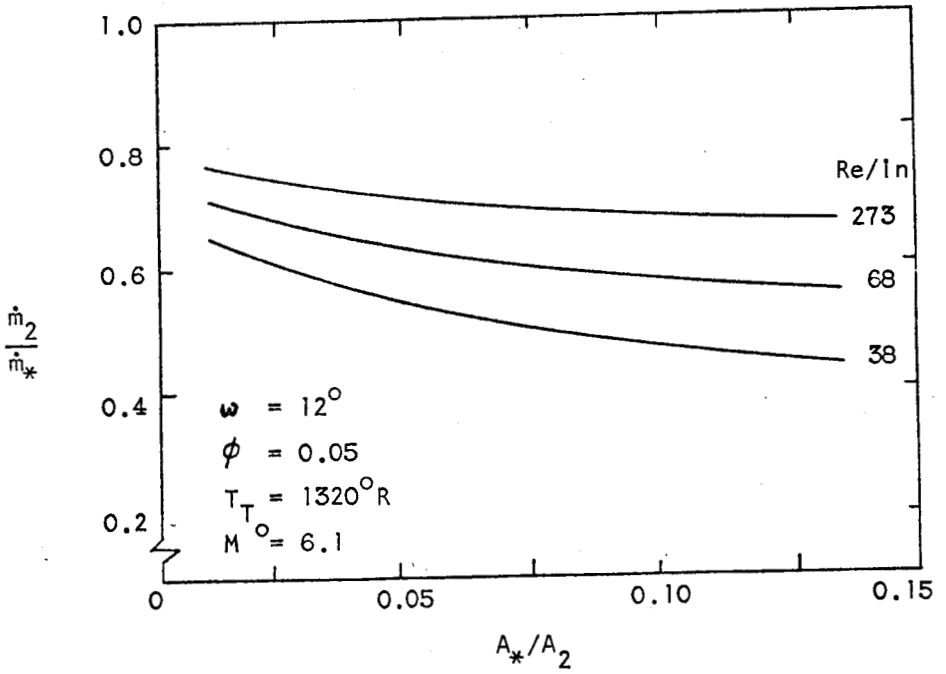

Figure 8. Variation of Diffuser Mass Flow with Reynolds No.

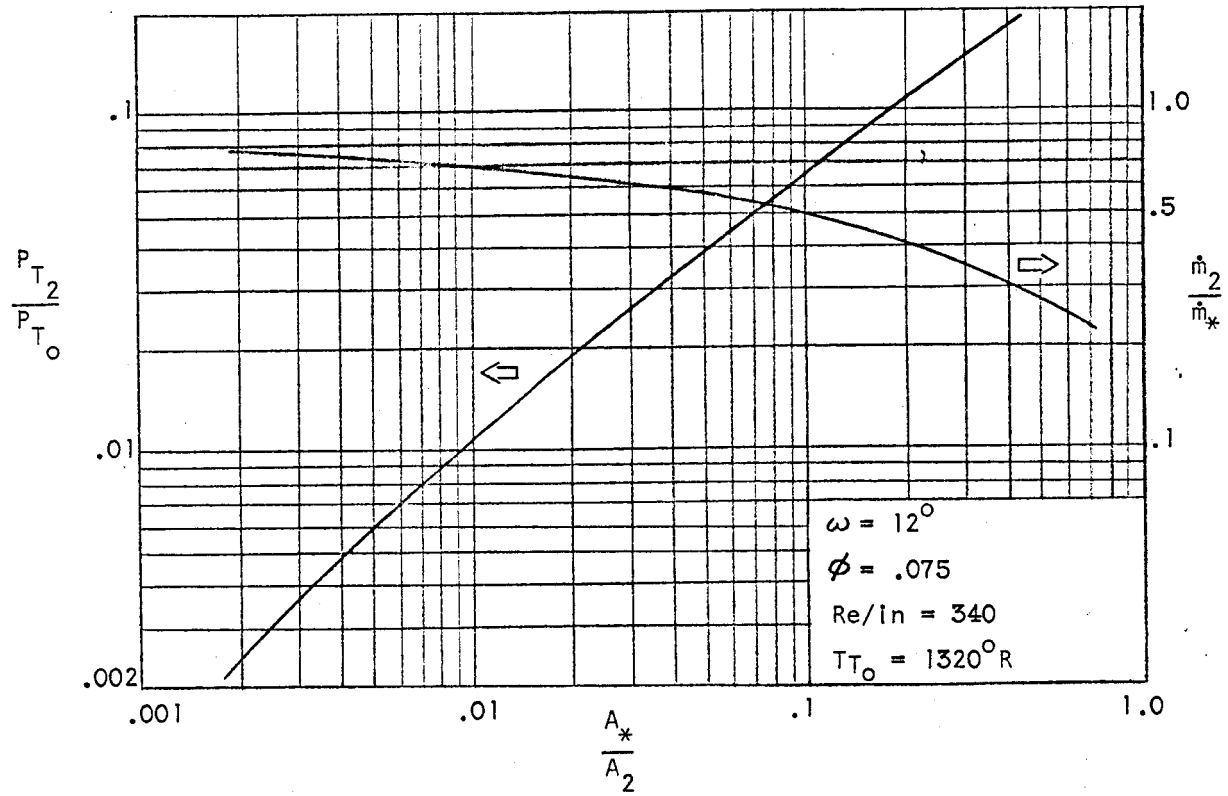

Figure 9. Variation of Pressure Recovery and Mass Flow with Area Ratio

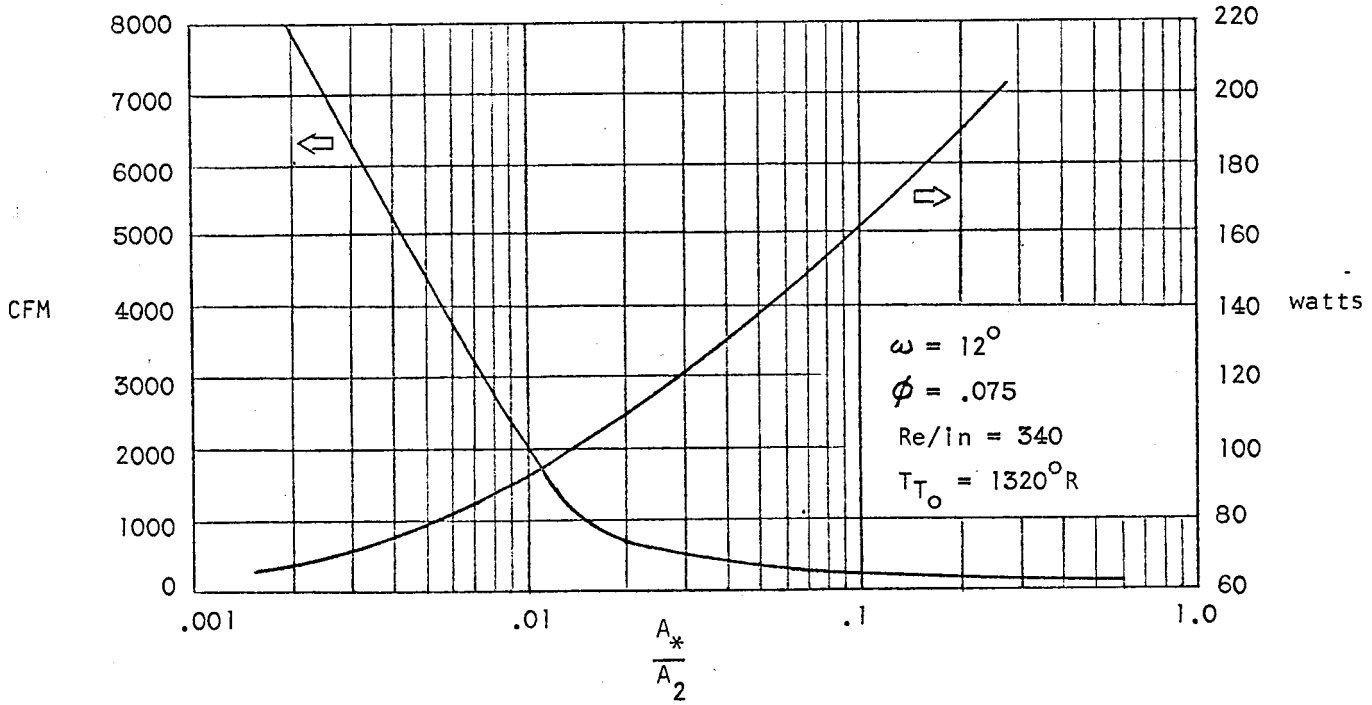

Figure 10. Variation of Pumping Requirements with Area Ratio

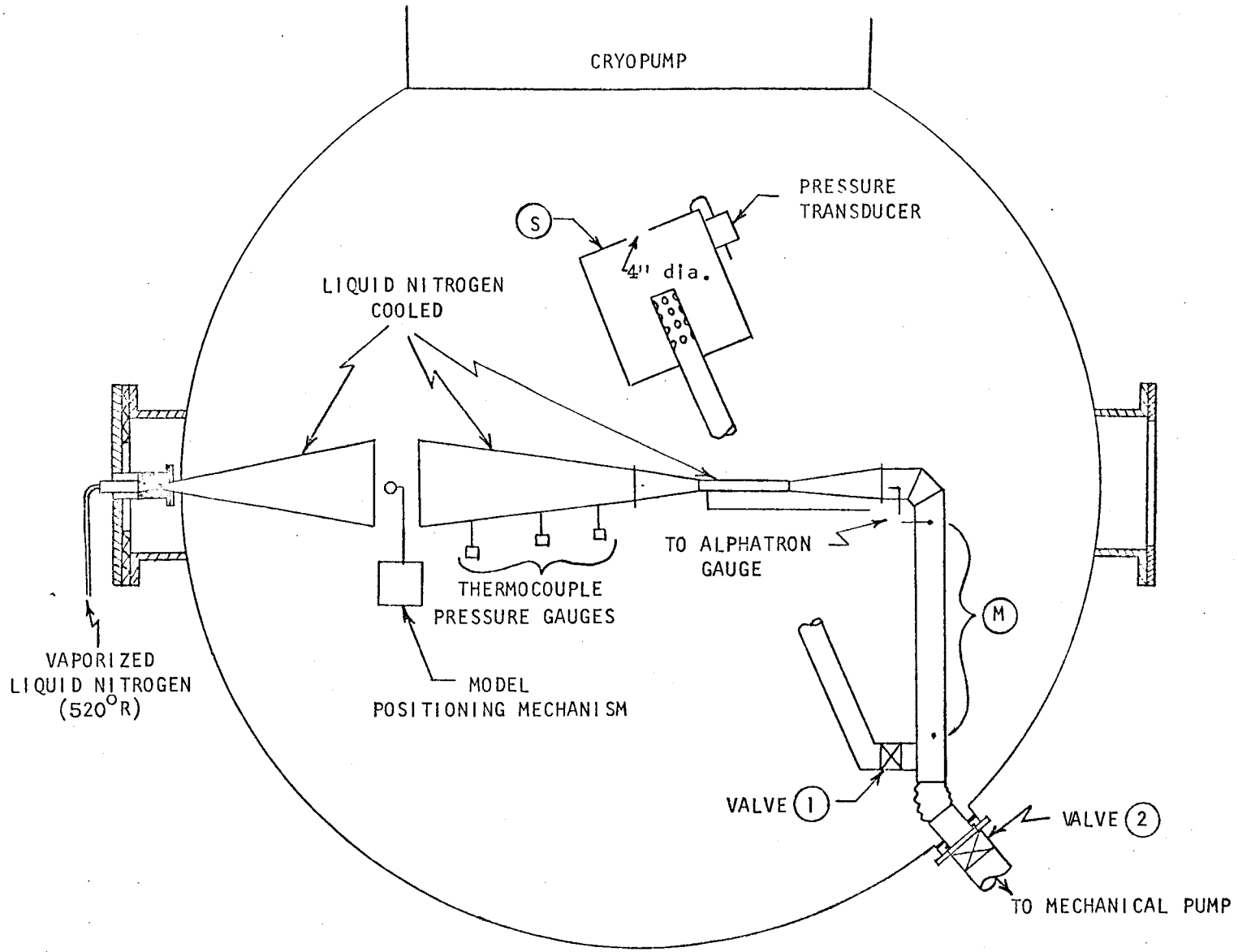

Figure 11. Experimental Arrangement

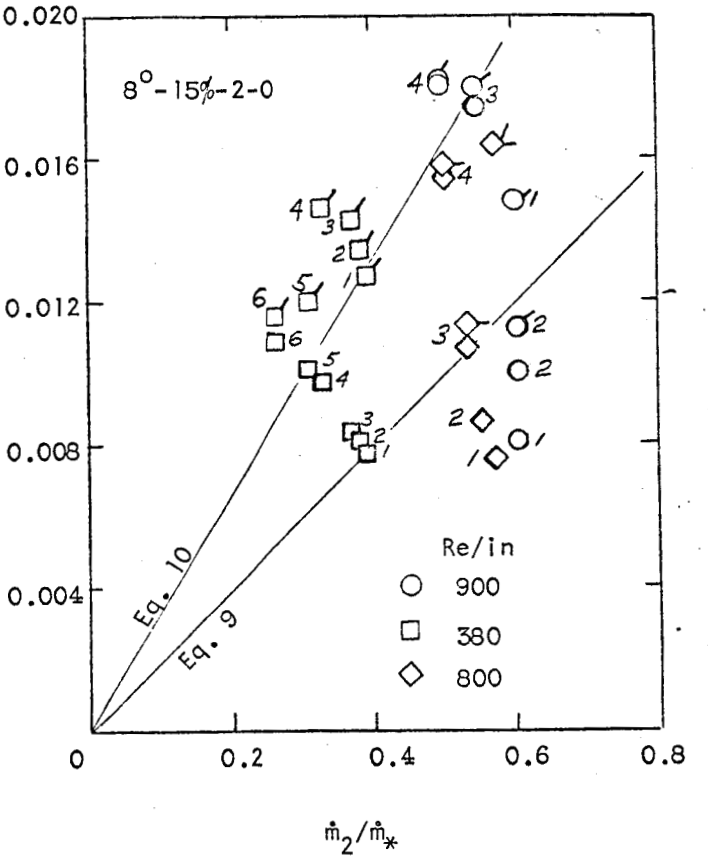

Figure 12. Variation of Pressure Recovery with Mass Flow

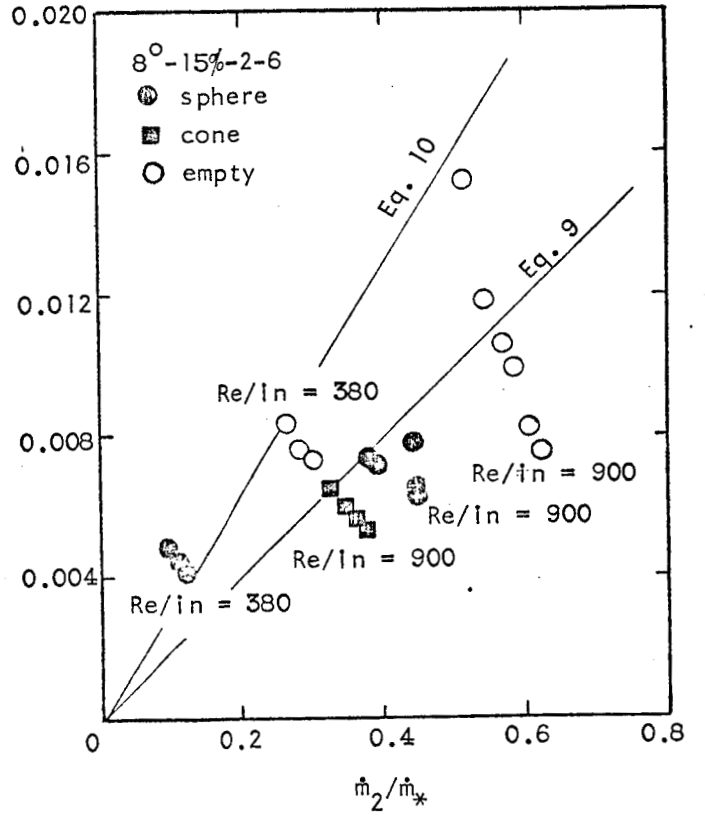

Figure 13. Variation of Pressure Recovery with Mass Flow

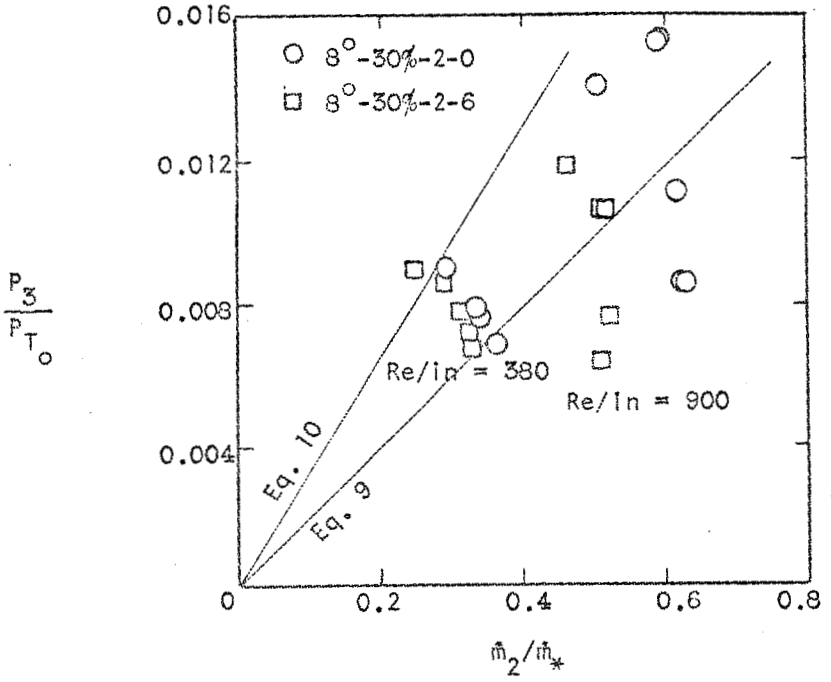

Figure 14. Variation of Pressure Recovery with Mass Flow

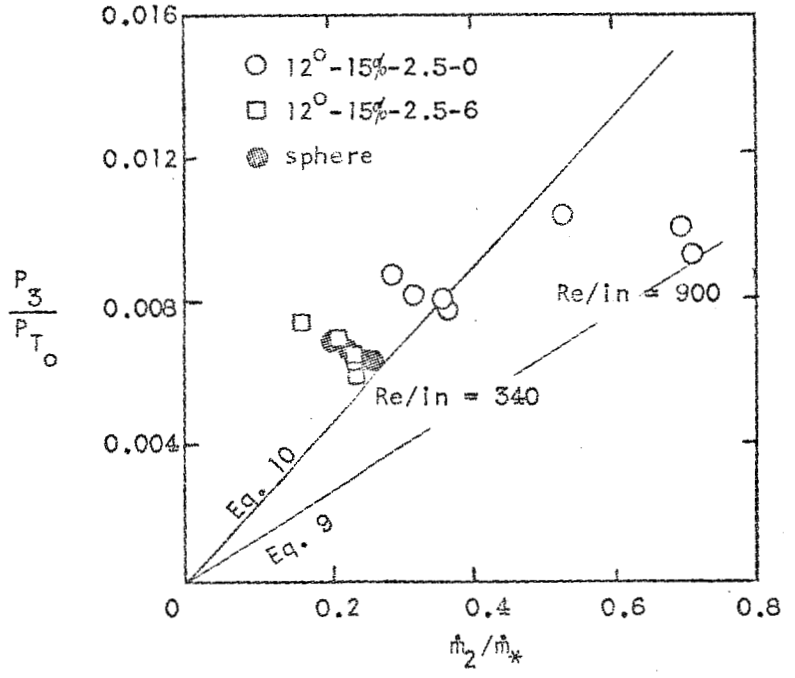

Figure 15. Variation of Pressure Recovery with Mass Flow

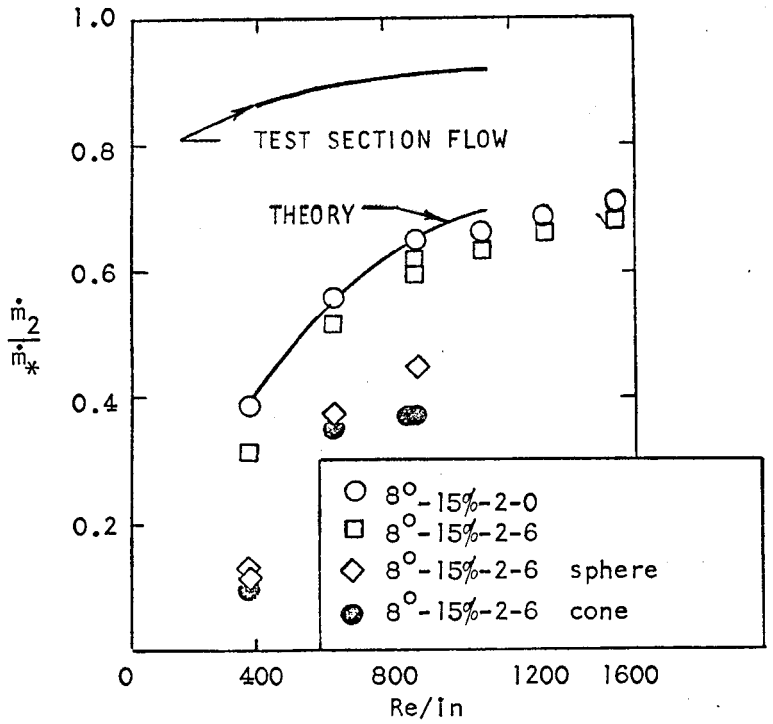

Figure 16. Variation of Mass Flow with Reynolds No.

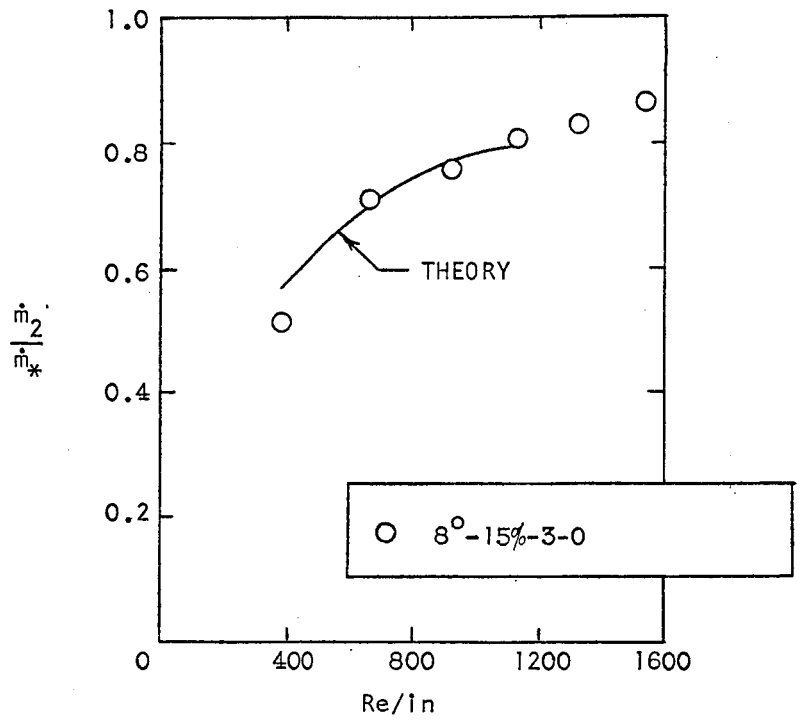

Figure 17. Variation of Mass Flow with Reynolds No.

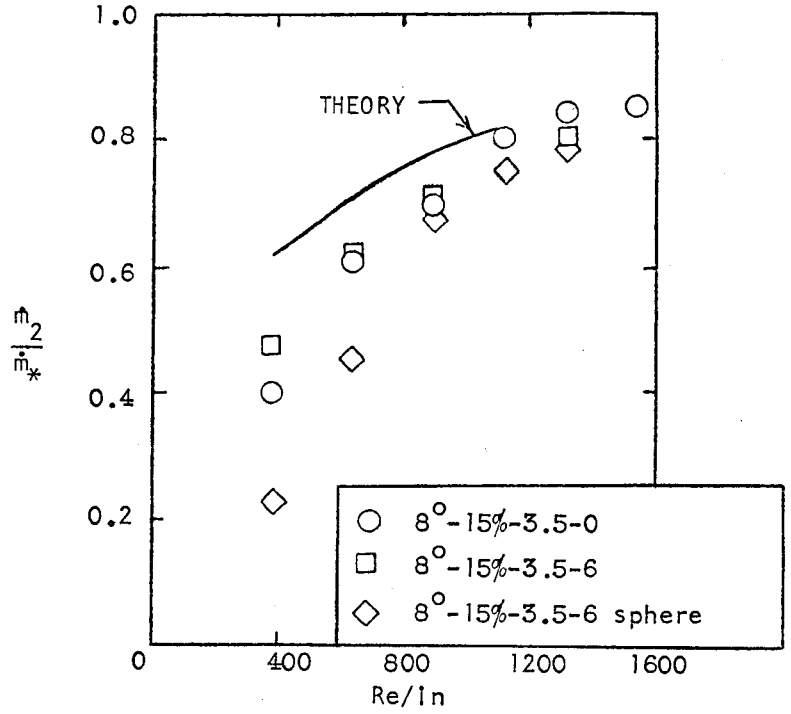

Figure 18. Variation of Mass Flow with Reynolds No.

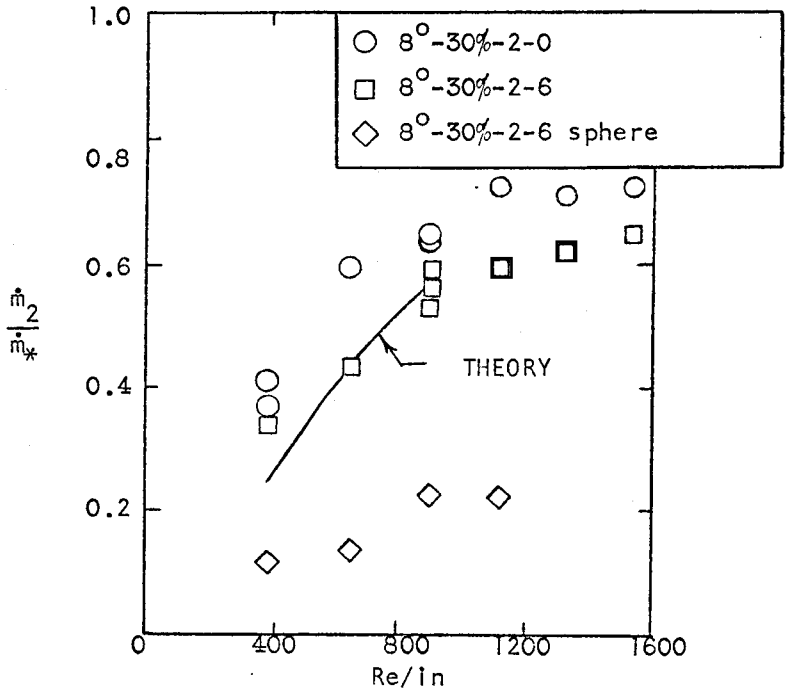

Figure 19. Variation of Mass Flow with Reynolds No.

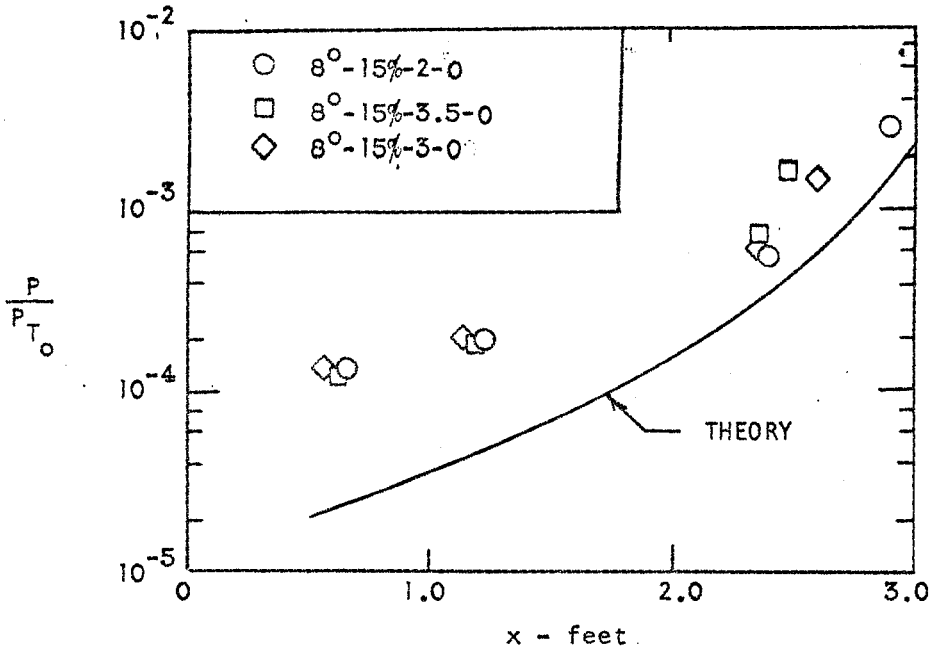

(a) Re/in = 900

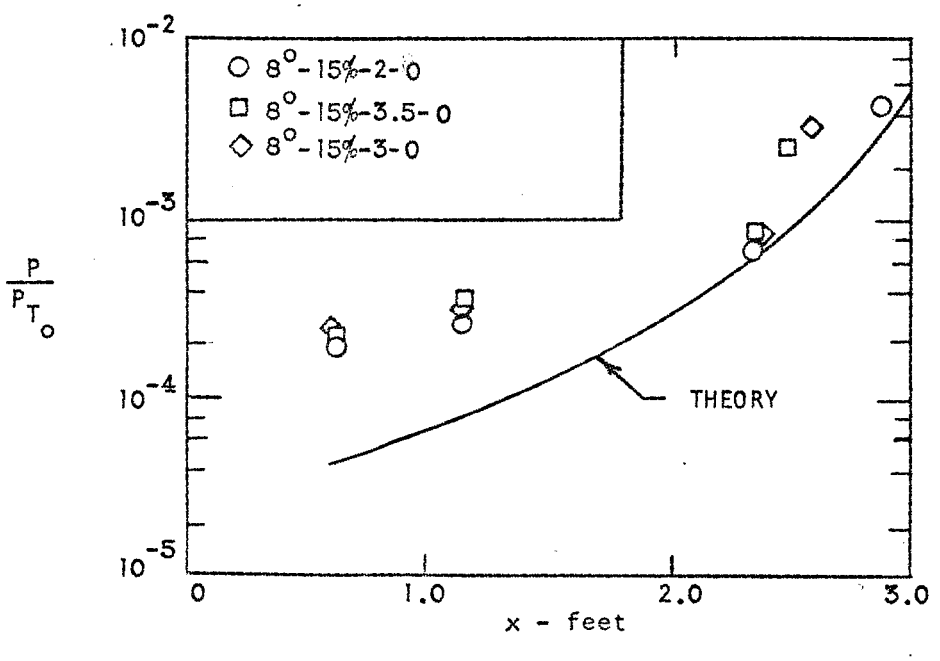

(b) Re/in = 380

Figure 20. Comparison Between Theoretical and Experimental Static Pressure Distribution

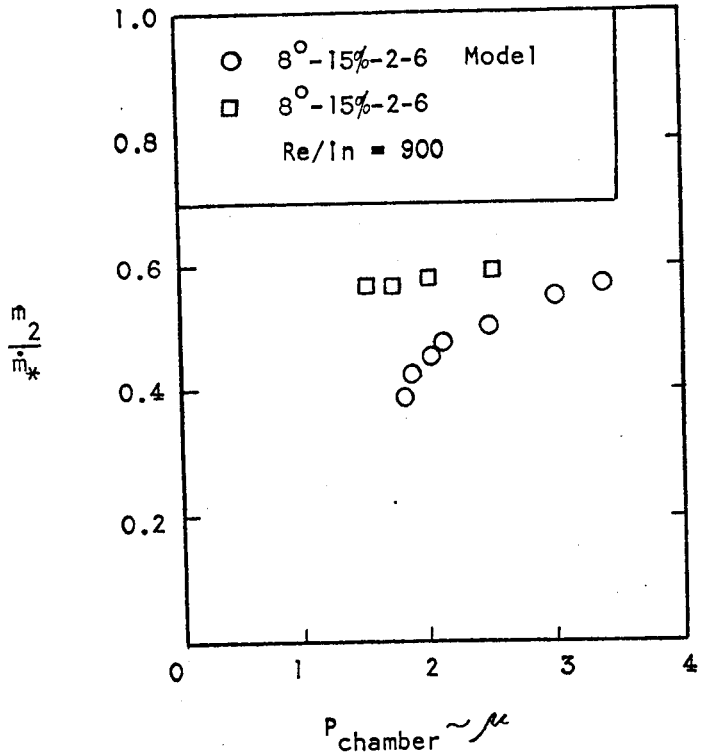

Figure 21. Variation of Mass Flow with Chamber Pressure

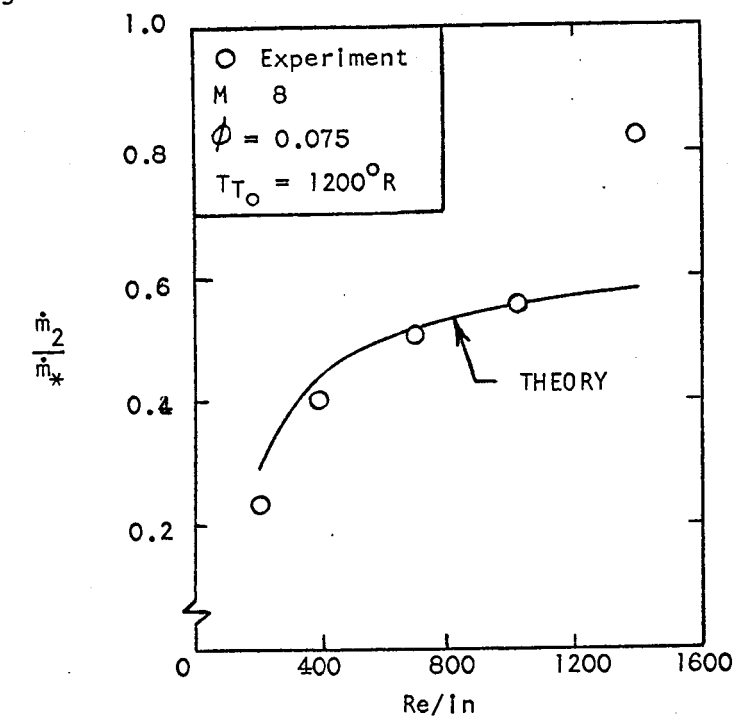

Figure 22. Comparison of Theoretical and Experimental Mass Flow

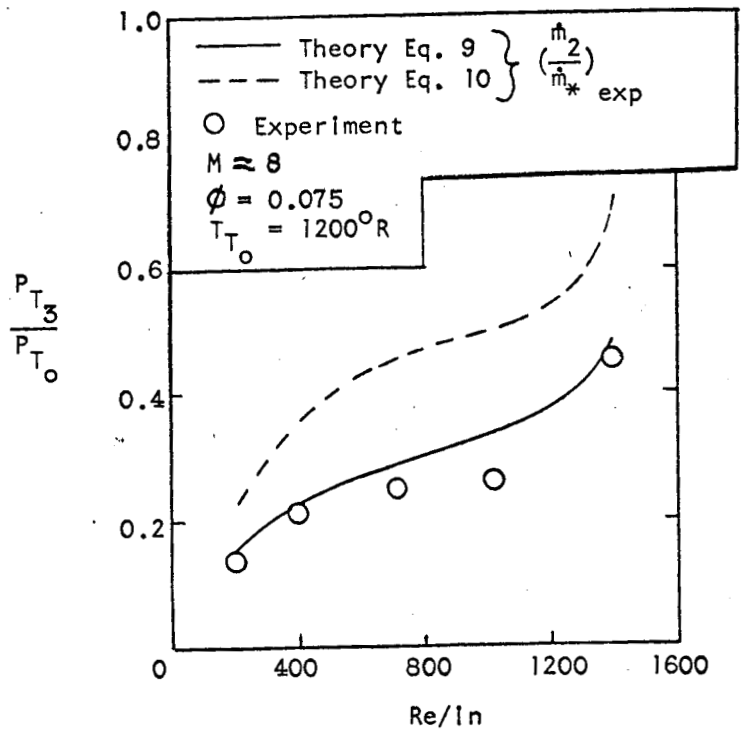

Figure 23 - Comparison of Theoretical and Experimental Pressure Recovery